# Synergistic tumor suppression by combined inhibition of telomerase and CDKN1A

Romi Gupta[a], Yuying Dong[a], Peter D. Solomon[a], Hiromi I. Wettersten[b], Christopher J. Cheng[c,d], JIn-Na Min[a,e], Jeremy Henson[f,g], Shaillay Kumar Dogra[h], Sung H. Hwang[i], Bruce D. Hammock[i], Lihua J. Zhu[j], Roger R. Reddel[f,g], W. Mark Saltzman[c], Robert H. Weiss[b,k], Sandy Chang[a,e], Michael R. Green[l,1], and Narendra Wajapeyee[a,1]

Departments of [a]Pathology and [e]Laboratory Medicine, Yale University School of Medicine, New Haven, CT 06510; [i]Department of Entomology and [b]Division of Nephrology, Department of Internal Medicine, University of California, Davis, California 95616; Departments of [c]Biomedical Engineering and [d]Molecular Biophysics and Biochemistry, Yale University, New Haven, CT 06511; [f]Sydney Medical School, University of Sydney, NSW 2006, Australia; [g]Cancer Research Unit, Children's Medical Research Institute, Westmead, NSW 2145, Australia; [h]Singapore Institute of Clinical Sciences, Agency for Science Technology and Research (A*STAR), Brenner Center for Molecular Medicine, Singapore 117609; [l]Howard Hughes Medical Institute and [j]Programs in Gene Function and Expression and Molecular Medicine, University of Massachusetts Medical School, Massachusetts 01605; and [k]Department of Medicine, Mather VA Medical Center, Sacramento, CA 9565

Contributed by Michael R. Green, June 19, 2014 (sent for review June 8, 2014)

**Tumor suppressor p53 plays an important role in mediating growth inhibition upon telomere dysfunction. Here, we show that loss of the p53 target gene cyclin-dependent kinase inhibitor 1A (*CDKN1A*, also known as *p21*$^{WAF1/CIP1}$) increases apoptosis induction following telomerase inhibition in a variety of cancer cell lines and mouse xenografts. This effect is highly specific to p21, as loss of other checkpoint proteins and CDK inhibitors did not affect apoptosis. In telomerase, inhibited cell loss of p21 leads to E2F1- and p53-mediated transcriptional activation of p53-upregulated modulator of apoptosis, resulting in increased apoptosis. Combined genetic or pharmacological inhibition of telomerase and p21 synergistically suppresses tumor growth. Furthermore, we demonstrate that simultaneous inhibition of telomerase and p21 also suppresses growth of tumors containing mutant p53 following pharmacological restoration of p53 activity. Collectively, our results establish that inactivation of p21 leads to increased apoptosis upon telomerase inhibition and thus identify a genetic vulnerability that can be exploited to treat many human cancers containing either wild-type or mutant p53.**

A prominent feature that distinguishes cancer cells from their normal counterparts is the expression of telomerase. Telomerase is a specialized ribonucleoprotein reverse transcriptase that synthesizes the telomeric DNA ends to maintain telomere length (1). During early tumorigenesis, telomerase expression is necessary to bypass replicative senescence, enabling immortalization of human cells (2). Notably, telomerase also represents an attractive target for cancer therapy because a large majority of cancer cells depend on telomerase expression for survival. Accordingly, genetic or pharmacological inhibition of telomerase has been shown to suppress growth of cancer cells (3). In fact, the telomerase inhibitor imetelstat, an oligonucleotide that inhibits telomerase activity by binding to the RNA component of human telomerase RNA (hTR), has advanced to the clinic for treatment of various hematological malignancies and solid tumors. To date, however, telomerase-based monotherapies have not been successful, underscoring the need to understand in greater detail how cancer cells respond to telomerase inhibition.

Previous studies have shown that the tumor suppressor p53 pathway plays a central role in regulating the cellular response to telomerase inhibition and telomere shortening (4). Genetic deletion of p53 in mice or RNA interference (RNAi)-mediated inhibition of p53 counteracts the growth suppression that occurs following telomerase inhibition. Furthermore, p53 loss cooperates with telomerase dysfunction to promote tumorigenesis (4). CDKN1A (also known as p21$^{WAF1/CIP1}$) is a cyclin-dependent kinase inhibitor and a direct transcriptional target of p53 (5, 6). p21 mediates several important physiological effects of p53, including DNA-damage–induced cell cycle checkpoints (7, 8). In addition to its role in cell cycle regulation, p21 has been shown in a variety of studies to repress apoptosis (9–13).

Here, we study the role of p21 in the context of telomerase inhibition. We find that abrogation of p21 function induces apoptosis in cancer cells following telomerase inhibition through up-regulation of p53-upregulated modulator of apoptosis (PUMA), a proapoptotic protein. Based upon these results, we go on to show that simultaneous genetic or pharmacological inhibition of telomerase and p21 can synergistically suppress tumor growth, even in p53 pathway-defective cancers.

## Results

**Induction of Apoptosis Following Telomerase Inhibition in Cancer Cells Lacking p21.** As described above, p53 is known to play an important role in the cellular response to telomere dysfunction, and *p21* is a major target of p53. However, the specific role of p21 in human cancer cells with dysfunctional telomeres has not been examined. Therefore, we asked whether cancer cells respond differently to telomerase inhibition and consequential telomere shortening in the presence or absence of p21. Toward this end, we treated HCT116 cells and HCT116 *p21* knockout cells (HCT116 p21KO) with the telomerase inhibitor imetelstat (14). We found that imetelstat inhibited proliferation of HCT116 p21KO cells

### Significance

**Over 90% of cancer cells express telomerase, which is required for their survival. However, telomerase inhibitors alone have so far failed to provide any significant clinical benefit. Therefore, identifying and targeting genes that can enhance the effects of telomerase inhibitors will greatly benefit a large population of cancer patients. We find that simultaneous inhibition of p21 and telomerase synergistically suppresses tumor growth. We also show that our approach is useful for treating p53 mutant cancers, when used with therapies that restore the function of mutant p53. We anticipate that simultaneous targeting of p21 and telomerase will overcome the current limitation of single-agent telomerase therapeutics and provide an effective method to treat cancers that rely on telomerase activity for survival.**

Author contributions: R.G. and N.W. designed research; R.G., Y.D., P.D.S., C.J.C., J.-N.M., and N.W. performed research; R.G., H.I.W., C.J.C., J.H., S.K.D., S.H.H., B.D.H., R.R.R., W.M.S., R.H.W., S.C., M.R.G., and N.W. contributed new reagents/analytic tools; R.G., Y.D., P.D.S., S.K.D., L.J.Z., S.C., M.R.G., and N.W. analyzed data; and R.G., M.R.G., and N.W. wrote the paper.

The authors declare no conflict of interest.

[1]To whom correspondence may be addressed. Email: Narendra.Wajapeyee@yale.edu or Michael.Green@umassmed.edu.

This article contains supporting information online at www.pnas.org/lookup/suppl/doi:10.1073/pnas.1411370111/-/DCSupplemental.

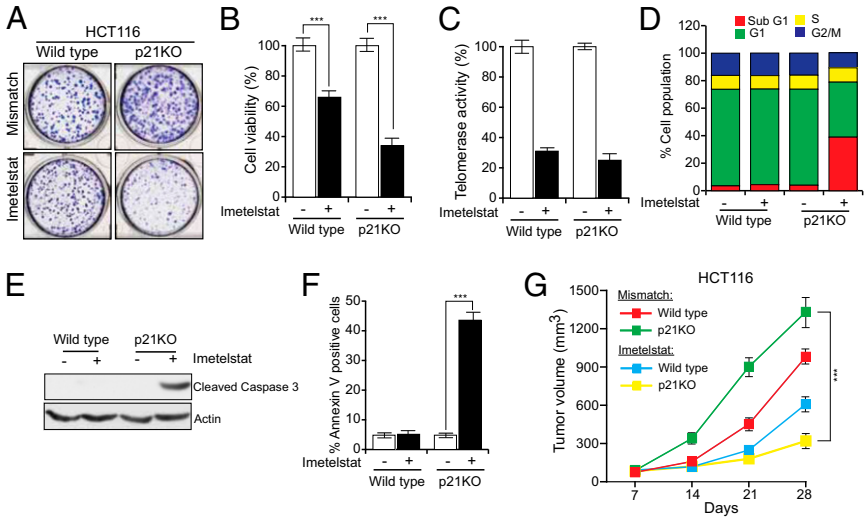


**Fig. 1.** Telomerase inhibition induces apoptosis in the absence of *p21*. Indicated cell lines were treated with mismatch oligonucleotide or imetelstat for 6 wk. (*A*) Crystal violet staining of HCT116 wild-type and p21KO colonies. Representative wells are shown. (*B*) Relative cell viability was monitored by trypan blue exclusion assay. (*C*) Telomerase activities of HCT116 wild-type and HCT116 p21KO cells. (*D*) Flow cytometry analysis to monitor apoptotic cells. (*E*) Cleaved caspase 3 immunoblot to measure apoptosis. Actin was used as a loading control. (*F*) % Annexin V–FITC–positive cells under indicated treatment conditions. (*G*) Average tumor volumes for indicated cell lines are presented at indicated conditions. ***$P < 0.0001$.

much more strongly than that of HCT116 cells (Fig. 1 *A* and *B*). Notably, telomerase inhibition in HCT116 and HCT116 p21KO cells was comparable (Fig. 1*C*). Additional experiments revealed that growth inhibition of HCT116 p21KO cells was largely due to increased apoptosis (Fig. 1 *D*–*F*). Furthermore, we knocked down telomerase using two different short hairpin RNAs (shRNAs) in HCT116 and HCT116 p21KO cells. Similar to the results with imetelstat, we found that shRNA-mediated knockdown of telomerase inhibited proliferation of HCT116 p21KO cells more efficiently than that of HCT116 cells (*SI Appendix*, Fig. S1).

Guided by these cell culture results, we injected HCT116 or HCT116 p21KO cells s.c. into athymic nude mice and monitored tumor growth after treatment with imetelstat or a control mismatch oligonucleotide. Similar to the cell culture results, we found that imetelstat inhibited growth of HCT116 p21KO tumors more effectively than that of HCT116 tumors (4.0-fold inhibition for HCT116 p21KO versus 1.6-fold inhibition for HCT116 cells) (Fig. 1*G*).

To determine the generality of these results, we used RNAi to knock down *p21* in HCT116 cells and the unrelated ACHN (renal) and RKO (colorectal) human cancer cell lines (*SI Appendix*, Figs. S2 and S3). Cells transduced with *p21* shRNAs or a nonspecific control shRNA were treated with imetelstat or a mismatch oligonucleotide and monitored for proliferation. As observed in HCT116 p21KO cells, shRNA-mediated knockdown of *p21* enhanced growth inhibition by imetelstat in HCT116, ACHN, and RKO cells by inducing apoptosis (*SI Appendix*, Fig. S2 and Fig. 2 *A*–*J*). In complete agreement with our cell culture experiments, we observed that treatment with imetelstat inhibited the growth of *p21* shRNA expressing ACHN and RKO tumors in mice much more strongly than ACHN and RKO tumors expressing a nonspecific control shRNA (Fig. 2 *K* and *L*).

We also analyzed the imetelstat sensitivity of four additional human cancer cell lines—LOX IMVI (melanoma), UACC62 (melanoma), CAKI (clear cell carcinoma), and NCI H460 (lung adenocarcinoma)—that express either high or low levels of p21. Similar to the results presented above, cell lines expressing a low level of p21 (NCI H460) were sensitive to imetelstat-mediated growth inhibition, whereas cell lines expressing a high level of p21 (LOX IMVI, UACC62, and CAKI) were not (*SI Appendix*, Fig. S3). In fact, proliferation of imetelstat-treated LOX IMVI and UACC62 cells was higher than that of the mismatch oligonucleotide-treated cells (*SI Appendix*, Fig. S3), possibly due to the activation of Alternative Lengthening of Telomeres (ALT) pathway (*SI Appendix*, Fig. S3). Taken together, these results indicate that loss of p21 sensitizes diverse cancer cell lines to tumor inhibition and apoptosis following abrogation of telomerase activity.

**Role of Other Checkpoint Proteins and Other CDK Inhibitors in Telomerase Inhibition-Induced Apoptosis.** p53 is necessary for DNA-damage–mediated transcriptional activation of *p21* (15), and genetic deletion of p21 abrogates p53-mediated G1 and G2/M checkpoints (8, 16). We therefore asked whether knockdown of other checkpoint proteins also sensitizes cancer cells to telomerase inhibition-mediated apoptosis. Toward this end, we analyzed two previously described checkpoint proteins, mediator of DNA damage checkpoint protein 1 (MDC1) and Nijmegen breakage syndrome 1 (NBS1) (17–19). Notably, MDC1 has been shown to have a role in detection and repair of human and mouse telomeres that are rendered dysfunctional through inhibition of TRF2 (20), whereas MRE11–RAD50–NBS1 has been shown to associate with TRF2 and human telomeres (21).

To test the effect of these proteins, *MDC1* and *NBS1* were knocked down in HCT116 cells, followed by treatment with imetelstat. As a control, HCT116 cells expressing a nonspecific shRNA were analyzed in parallel. In contrast to the results with *p21*, depletion of NBS1 or MDC1 did not increase the sensitivity of HCT116 cells to imetelstat-mediated growth suppression (*SI Appendix*, Fig. S4).

Additionally, we also tested the role of a second cyclin-dependent kinase inhibitor CDKN1B (also known as p27). In contrast to p21 loss, knockdown of *p27* did not sensitize HCT116 cells to imetelstat-induced apoptosis (*SI Appendix*, Fig. S5). Furthermore, although the cancer cell lines used in our studies lacked *CDKN2A* (also known as p16) (*SI Appendix*, Table S1) (22, 23), they varied in their response to imetelstat. These results indicate that p16 expression also does not determine the response of cancer cells to telomerase inhibition. Collectively, these results show that unlike p21, loss of other checkpoint proteins (e.g., MDC1 and NBS1) or other CDK inhibitors (e.g., p27 and p16) does not cooperate with imetelstat to induce apoptosis.

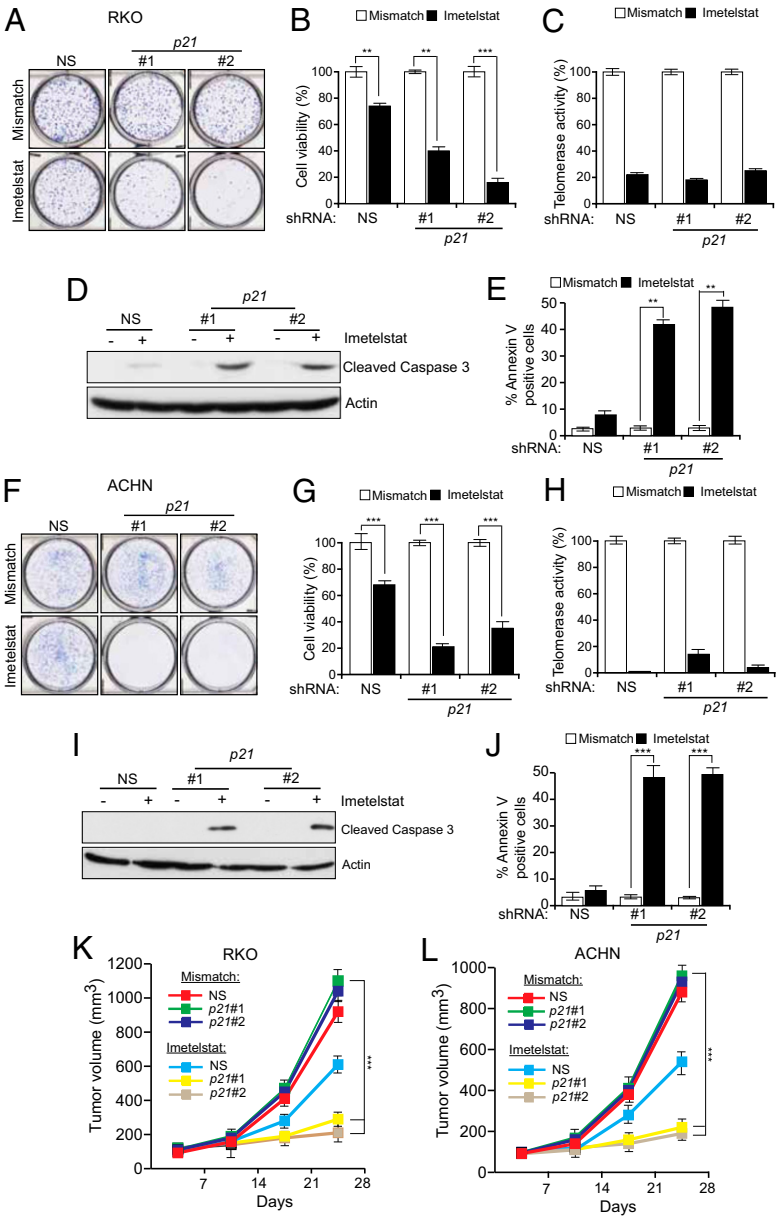


**Fig. 2.** shRNA-mediated *p21* knockdown in unrelated human cancer cell lines sensitizes them to telomerase inhibition-mediated apoptosis. Analysis of RKO (*A–E*) and ACHN (*F–J*) cells stably transduced with nonspecific control (NS) or two different *p21* shRNAs. (*A–E* and *F–J*) Cells were treated with mismatch oligonucleotide or with imetelstat for 6 wk. (*A* and *F*) Colony formation monitored by crystal violet staining. (*B* and *G*) Cell viability was measured by trypan blue exclusion assay. Cell viability relative to mismatch oligonucleotide is plotted. (*C* and *H*) Telomerase activity as measured by the TRAP assay and plotted relative to the mismatch oligonucleotide. (*D* and *I*) Cleaved caspase 3 immunoblot to measure apoptosis. Actin was used as a loading control. (*E* and *J*) % Annexin V–FITC–positive cells under indicated treatment conditions. (*K* and *L*) Average tumor volumes for indicated cell lines for indicated conditions are shown. $^{**}P < 0.001$; $^{***}P < 0.0001$.

We also tested whether a general cellular stress could cooperate with either imetelstat treatment or p21 loss to induce apoptosis. Our results show that tunicamycin, which induces ER stress, had no cooperative effect with either imetelstat treatment or p21 loss on cell proliferation or apoptosis (*SI Appendix*, Fig. S6).

**Apoptosis Induction After Telomerase Inhibition in Cancer Cells Lacking p21 Does Not Involve Telomere Attrition or ALT.** We next sought to understand the mechanism by which apoptosis is induced by imetelstat in HCT116 p21KO cells. First, we examined whether loss of p21 affects the ability of imetelstat to induce telomere shortening. *SI Appendix*, Fig. S7 *A–D* shows that there was no significant difference between imetelstat-treated HCT116 and HCT116 p21KO cells in either the extent of telomere shortening or the number of signal-free chromosomal ends. Although in most cancer cells maintenance of telomere length depends on telomerase activity, in about 10–15% of cancers telomere length is maintained through an alternative ALT pathway (24). The mechanism of ALT has not been fully elucidated, however a general consensus is that it requires homologous recombination (24). Furthermore, previous studies have shown that, following telomerase inhibition, cancer cells can survive by activating the ALT pathway (24, 25). We therefore tested whether the ALT pathway was more active in HCT116 cells than HCT116 p21KO cells after imetelstat treatment by monitoring partially single-stranded telomeric $(CCCTAA)_n$ DNA circles (C-circles), a characteristic, quan-

tifiable marker of ALT activity (26). As expected, the previously described ALT-positive osteosarcoma cell line U2OS produced C-circles, whereas ALT-negative HeLa cells did not (*SI Appendix*, Fig. S7*E*). Notably, we did not detect C-circles in either HCT116 or HCT116 p21KO cells, before or after imetelstat treatment, indicating that ALT activity does not explain the differential response to imetelstat. As an additional control, we analyzed the effect of telomerase inhibition in cancer cell line U2OS, in which the ALT pathway is active, and thus these cells do not depend upon telomerase expression for survival (27). As expected, treatment with imetelstat did not affect the proliferation of U2OS cells in the absence or presence of *p21* shRNAs (*SI Appendix*, Fig. S8). Collectively, these results further confirm that imetelstat inhibits telomerase activity to prevent growth of cancer cells that are dependent upon telomerase activity for survival.

**P53- and E2F1-Mediated PUMA Activation in Cells Lacking p21 After Telomerase Inhibition.** In addition to promoting cell cycle arrest in response to DNA damage, the tumor suppressor p53 activates proapoptotic genes such as *BAX*, *BAK*, and *PUMA* to induce apoptosis (28–32). We therefore monitored expression of *BAX*, *BAK*, and *PUMA* in HCT116 and HCT116 p21KO cells treated with imetelstat. Unexpectedly, imetelstat treatment induced *PUMA* expression to substantially higher levels in HCT116 p21KO cells compared with HCT116 cells (Fig. 3 *A* and *B*). Likewise, shRNA-mediated knockdown of *p21* in RKO and ACHN cells led to a large increase in PUMA expression following imetelstat treatment (*SI Appendix*, Fig. S9 *A* and *B* as well as *G* and *H*). By contrast, following imetelstat treatment, *BAK* expression was actually higher in HCT116 cells than in HCT116 p21KO cells, and *BAX* expression was comparable in the two cell lines (Fig. 3 *A* and *B*).

Previous studies have shown that the E2F1 transcription factor is an activator of *PUMA* transcription and that p21 can negatively regulate E2F1 activity (33, 34). These two findings suggested that E2F1 might activate *PUMA* expression in HCT116 p21KO cells following imetelstat treatment. Consistent with this idea, following knockdown of *E2F1* in HCT116 p21KO cells, imetelstat treatment no longer activated *PUMA* expression (Fig. 3 *C* and *D*). Furthermore, following shRNA-mediated knockdown of *E2F1* in HCT116 p21KO cells, imetelstat failed to inhibit cellular proliferation (Fig. 3*E* and *SI Appendix*, Fig. S10) or efficiently induce apoptosis (Fig. 3 *F* and *G*). Likewise, *PUMA* transcription was not activated by imetelstat in HCT116 p53KO cells following *p21* knockdown (Fig. 3 *H* and *I*). *PUMA* expression was comparable in imetelstat-treated cells containing or depleted of the checkpoint proteins *NBS1* and *MDC1* (*SI Appendix*, Fig. S4 *F* and *L*) as well as in cells depleted of the CDK inhibitor p27 (*SI Appendix*, Fig. S5*F*), again confirming the specific role of p21 in regulating apoptosis following telomerase inhibition. Thus, in the absence of p21, E2F1 and p53 activate *PUMA* expression in telomerase-inhibited cells.

Previous work has shown that p53 deficiency prevents the growth inhibitory effects of telomere dysfunction (35). Indeed, we found that HCT116 p53KO cells were more resistant to

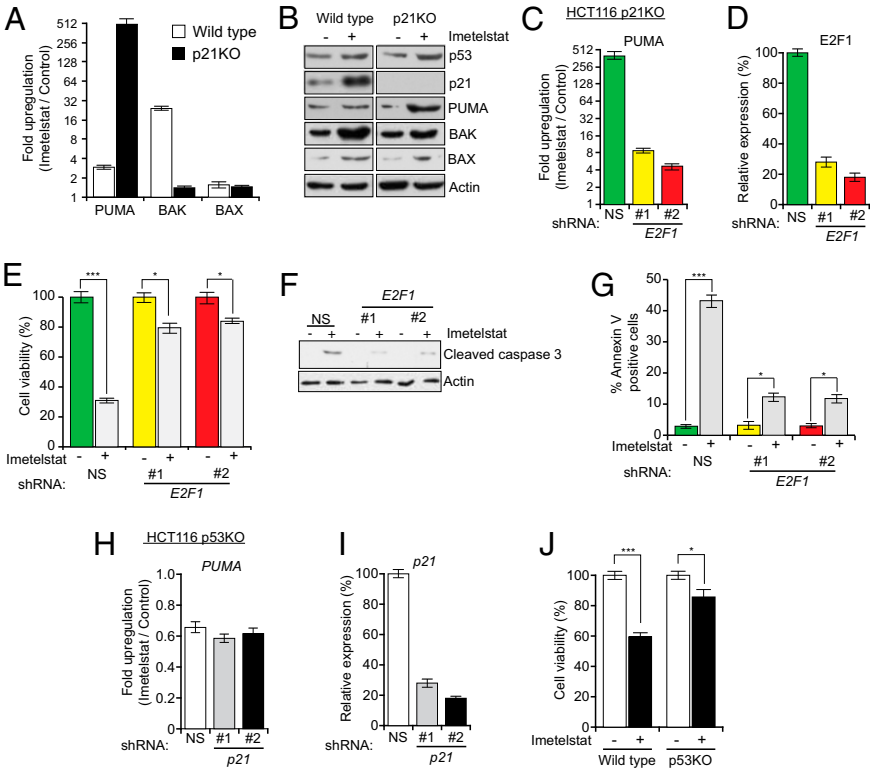


**Fig. 3.** Telomerase inhibition activates E2F1- and p53-dependent *PUMA* transcription in the absence of *p21*. Indicated cell lines were treated with either a mismatch oligonucleotide or imetelstat. (*A*) Fold change in *PUMA*, *BAK*, and *BAX* transcript levels measured by quantitative RT-PCR (qRT-PCR) after 6 wk of treatment. (*B*) Immunoblot analysis was performed for indicated proteins. (*C*) *PUMA* expression was measured in imetelstat-treated HCT116 p21KO cells after *E2F1* or control (NS) shRNA knockdown. (*D*) *E2F1* knockdown was confirmed by qRT-PCR. (*E*) Relative cell viability was measured by trypan blue exclusion assay. (*F*) Cleaved caspase 3 was measured by immunoblot in mismatch oligonucleotide or imetelstat-treated HCT116 p21KO cells after *E2F1* or control (NS) shRNA knockdown. Actin expression was monitored as a control. (*G*) Annexin V–FITC–positive cells were quantified by FACS analysis in mismatch oligonucleotide or imetelstat-treated HCT116 p21KO cells after *E2F1* or control (NS) shRNA knockdown. (*H*) *PUMA* expression in imetelstat-treated HCT116 p53KO after *p21* or control (NS) shRNA knockdown. (*I*) *p21* knockdown was confirmed by qRT-PCR. (*J*) Cell viability of HCT116 wild-type and p53KO cells after 6 wk of imetelstat treatment monitored by trypan blue exclusion. $*P < 0.01$; $***P < 0.0001$.

imetelstat than parental HCT116 cells (Fig. 3*J* and *SI Appendix*, Fig. S10). These results led us to hypothesize that p53- and E2F1-dependent activation of *PUMA* transcription is necessary for apoptosis induction following telomerase inhibition in p21KO cells. To test this idea, we used an HCT116 cell line bearing homozygous deletions in both *p21* and *PUMA* (HCT116 *p21*/*PUMA* DKO). Notably, loss of *PUMA* prevented growth inhibition and apoptosis following treatment of HCT116 p21KO cells with imetelstat (Fig. 4 *A*–*C*). Likewise, simultaneous shRNA-mediated knockdown of *PUMA* (*SI Appendix*, Fig. S9 *C* and *I*) counteracted imetelstat-mediated growth inhibition in RKO and ACHN cells expressing a *p21* shRNA (*SI Appendix*, Fig. S9 *D*–*F* and *J*–*L*).

To test whether loss of *PUMA* also rescued imetelstat-mediated growth inhibition in vivo, we injected HCT116, HCT116 p21KO, and HCT116 p21/PUMA DKO cells into the flanks of nude mice followed by treatment with either imetelstat or a mismatch oligonucleotide. Consistent with the cell culture results, imetelstat did not suppress growth of tumors lacking both *p21* and *PUMA* (Fig. 4*D*). Analysis of tumors by terminal deoxynucleotidyl transferase-mediated dUTP nick end labeling (TUNEL) showed that after imetelstat treatment, apoptosis was significantly higher in p21KO tumors compared with HCT116 p21/PUMA DKO tumors (Fig. 4 *E* and *F*). Collectively, these results demonstrate that in the absence of *p21*, telomerase inhibition leads to E2F1- and p53-dependent transcriptional activation of *PUMA*, resulting in apoptosis.

To establish the generality of the *PUMA* transcriptional activation mechanism, we analyzed five human cancer cell lines with differing levels of p21 expression. We found that in a cell line with low p21 levels (NCI H460) transcriptional activation of *PUMA* after imetelstat treatment was substantially higher than that of cell lines with high p21 levels (LOX IMVI, UACC62, and CAKI; *SI Appendix*, Fig. S11*A*). Furthermore, knockdown of *PUMA* (*SI Appendix*, Fig. S11*B*) rescued NCI H460 cells from imetelstat-mediated growth inhibition (*SI Appendix*, Fig. S11 *C* and *D*). Collectively, these results show that activation of *PUMA* is necessary for apoptosis induction in cells lacking p21 after telomerase inhibition.

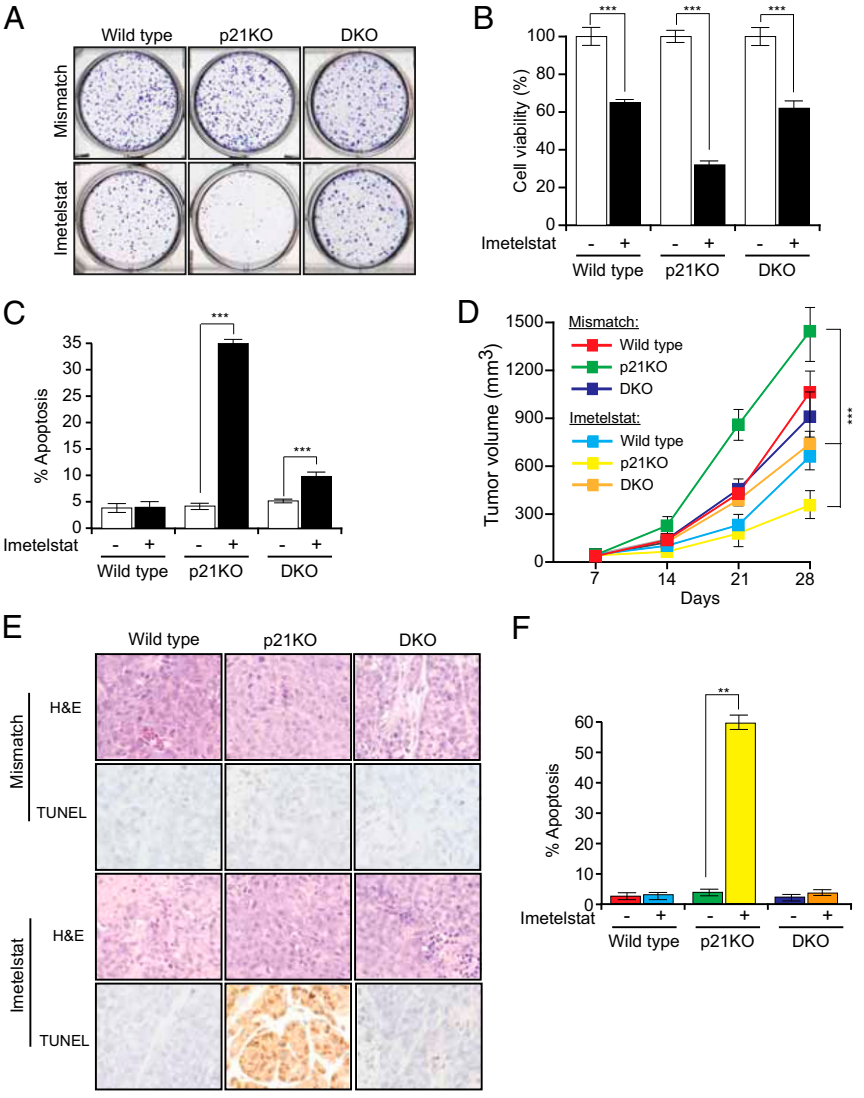


**Fig. 4.** PUMA induces apoptosis when telomerase is inhibited in the absence of *p21*. Indicated cell lines were treated with either a mismatch oligonucleotide or imetelstat for 6 wk. (*A*) Crystal violet staining of HCT116 wild-type, p21KO, and p21/PUMA DKO colonies. Representative wells are shown. (*B*) Relative cell viability of the indicated cells measured by trypan blue exclusion assay. (*C*) Apoptosis was measured by FACS analysis. (*D*) Average tumor volumes from mice treated with either mismatch oligonucleotide or imetelstat for indicated conditions for noted cell lines are shown. (*E*) TUNEL assay measuring apoptosis for indicated tumor samples was performed. (*F*) Quantitation of TUNEL-positive cells is shown. $^{**}P < 0.001$; $^{***}P < 0.0001$.

**Synergistic Tumor Suppression by RNAi-Mediated p21 Depletion and Imetelstat Treatment.** The results described above suggested that simultaneous inhibition of p21 and telomerase could synergistically suppress tumor growth. We therefore carried out a series of experiments in which p21 function was abrogated using different approaches and telomerase was inhibited with imetelstat. In the first approach, we used a polymer nanoparticle-based system to deliver a *p21* small interfering RNA (siRNA) (36, 37). These poly(lactic-*co*-glycolic acid) (PLGA) nanoparticles were coated with the PEGylated cell-penetrating peptide, N terminus of the CPP penetratin (ANTP), and loaded with a p21 siRNA. As a control, a nonspecific negative control siRNA was similarly encapsulated into modified PLGA nanoparticles. We then s.c. injected HCT116 and ACHN cells into athymic nude mice and systemically treated the mice with imetelstat and nanoparticles encapsulated in siRNA. In good agreement with our cell culture results, the combination of a p21 siRNA and imetelstat resulted in significantly stronger tumor suppression compared with imetelstat alone (*SI Appendix*, Fig. S12 *A* and *B* and Table S2). Furthermore, as expected, analyses of tumor lysates revealed reduced p21 expression in *p21* siRNA nanoparticle-injected tumors (*SI Appendix*, Fig. S12 *C* and *D*), increased apoptosis upon simultaneous inhibition of p21 and telomerase (*SI Appendix*, Fig. S12 *C* and *D*), and reduced telomerase activity in imetelstat-treated tumor samples (*SI Appendix*, Fig. S12 *E* and *F*).

**Synergistic Tumor Suppression by Pharmacological Inhibition of Telomerase and p21.** The *p21* siRNA results described above provide proof-of-principle that systemic in vivo targeting of p21 can substantially enhance tumor suppression when combined with telomerase inhibition. We next performed experiments in which p21 function was abrogated by pharmacological inhibition in conjunction with imetelstat treatment. We first inhibited p21 expression in HCT116 cells using sorafenib (Fig. 5*A*), which promotes proteasome-mediated degradation of p21 (38). As predicted, we found that sorafenib sensitized cells to imetelstat-mediated growth inhibition and apoptosis induction (Fig. 5 *B–D*). Notably, reintroduction of *p21* in HCT116 cells treated with imetelstat and sorafenib substantially counteracted growth inhibition and apoptosis induction (Fig. 5 *E–H*), confirming that sorafenib functions by down-regulating p21 activity. Next, we tested the combined effect of imetelstat and sorafenib in suppressing tumor growth in mouse xenografts. We found that simultaneous treatment with imetelstat and sorafenib was substantially more effective at suppressing growth of HCT116 xenografts than either drug alone and thus functions in a synergistic manner (Fig. 5*I* and *SI Appendix*, Table S2).

Toxicity analyses revealed that there were no significant differences in the body weight or alanine aminotransferase (ALT), aspartate aminotransferase (AST), alkaline phosphatase (AP), whole blood counts, and renal activity markers in mice that were treated with imetelstat sorafenib, or both, in comparison with the control group (*SI Appendix*, Fig. S13). Finally, to determine the generality of these results, we analyzed the effect of combined imetelstat and sorafenib treatment on xenografts formed from five additional human cancer cell lines representing four different tissue origins. Notably, in all cases, treatment with both imetelstat and sorafenib was substantially more effective at suppressing tumor growth than either drug alone (*SI Appendix*, Fig. S14 and Table S2).

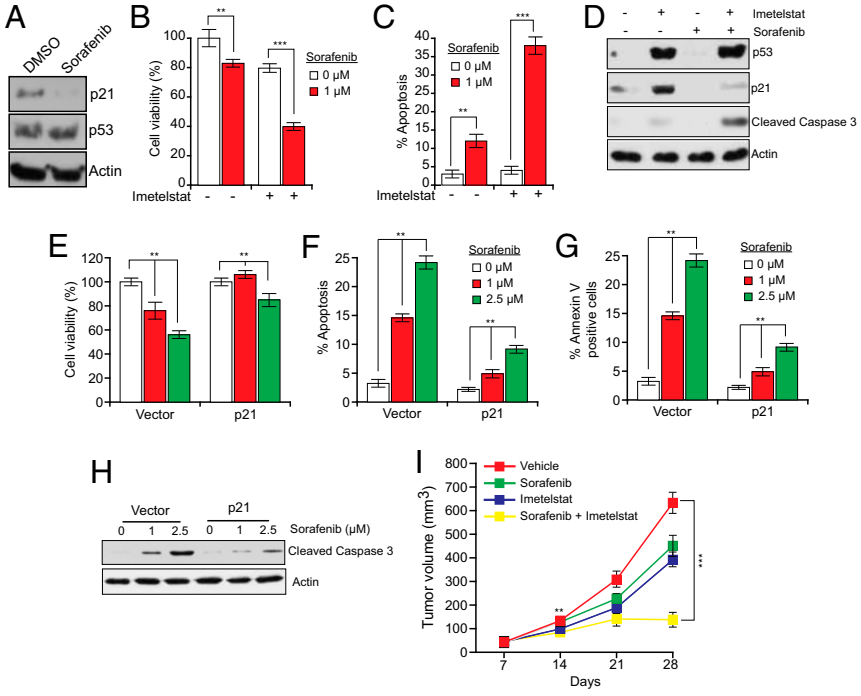


**Fig. 5.** Simultaneous pharmacological inhibition of p21 by sorafenib and telomerase prevents tumor growth in mice. (*A*) Immunoblot of p21 expression in HCT116 cells treated with DMSO or sorafenib (1 μM) for 24 h. (*B*) Relative cell viability measured by trypan blue exclusion assay of HCT116 cells treated with imetelstat and sorafenib. (*C*) Apoptosis of HCT116 cells treated with imetelstat and sorafenib was measured by FACS analysis. (*D*) Immunoblot for indicated proteins in HCT116 cells treated with sorafenib, imetelstat, or both. (*E*) Relative cell viability measured by trypan blue exclusion assay of imetelstat-treated HCT116 cells transfected with control or *p21* expression vectors and then treated with sorafenib. (*F*) Apoptosis measured by FACS analysis of imetelstat-treated HCT116 cells transfected with control or *p21* expression vectors and then treated with sorafenib. (*G*) Annexin V–FITC–positive cells were quantified by FACS analysis of imetelstat-treated HCT116 cells transfected with control or *p21* expression vectors and then treated with sorafenib. (*H*) Cleaved caspase 3 was measured by immunoblot in imetelstat-treated HCT116 cells transfected with control or *p21* expression vectors and then treated with sorafenib. (*I*) Average tumor volumes from mice treated with vehicle, sorafenib alone, imetelstat alone, or both drugs. $^{**}P < 0.001$; $^{***}P < 0.0001$.

Sorafenib has been shown to have cellular targets other than p21, including BRAF and VEGF (39). Therefore, we asked whether an alternative pharmacological inhibitor that more selectively targets p21 expression can, like sorafenib, cooperate with imetelstat to suppress tumor growth. Toward this end, we used a recently identified pharmacological p21 inhibitor, UC2288 (Fig. 6*A*), which down-regulates p21 levels through transcriptional and post-transcriptional mechanisms (40). Furthermore, unlike Sorafenib, UC2288 does not inhibit RAF kinase or VEGF activities (40). In agreement with previous studies, we observed that treatment of cancer cells with UC2288 led to decreased p21 levels (Fig. 6*B*). Furthermore, whereas UC2288 alone had only modest growth inhibitory effects, combining UC2288 with imetelstat potently inhibited cancer cell growth by inducing apoptosis (Fig. 6 *C*–*E*). The ability of UC2288 to inhibit growth was largely dependent upon its ability to down-regulate p21 expression, because ectopic expression of *p21* counteracted growth inhibition and apoptosis induction in UC2288 and imetelstat-treated cancer cells (Fig. 6 *F*–*H*). Finally, we tested whether UC2288 can inhibit tumor growth in vivo. Toward this end, we injected HCT116 and ACHN cells

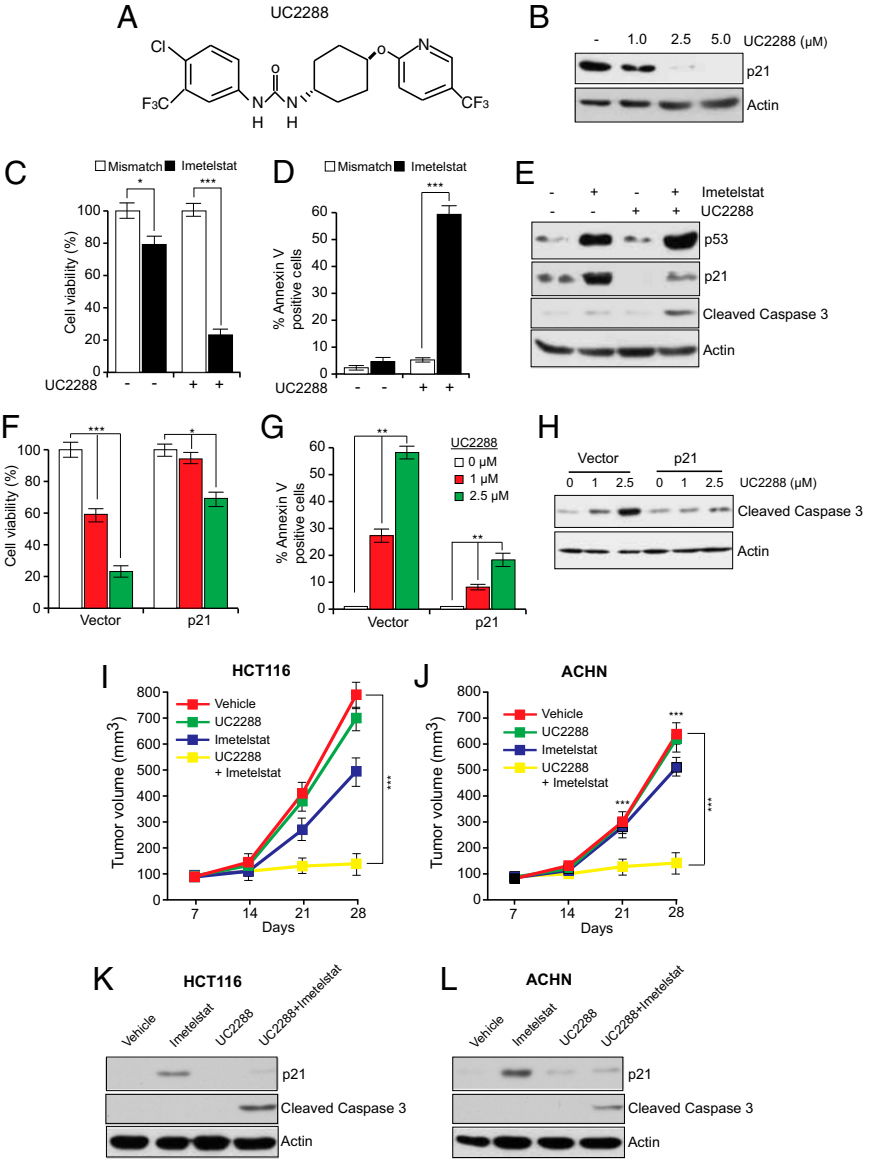


**Fig. 6.** Simultaneous pharmacological inhibition of p21 by UC2288 and telomerase prevents tumor growth in mice. (*A*) Chemical structure of UC2288. (*B*) Immunoblot of p21 expression in HCT116 cells treated with DMSO or with indicated concentrations of UC2288 for 24 h. (*C*) Relative cell viability measured by trypan blue exclusion assay of HCT116 cells treated with imetelstat, UC2288 (2.5 μM), or both. (*D*) % Annexin V–FITC–positive HCT116 cells treated with imetelstat and UC2288 was measured by FACS analysis. (*E*) Immunoblot for indicated proteins in HCT116 cells following treatment with U2288, imetelstat, or both. (*F*) Relative cell viability measured by trypan blue exclusion assay of imetelstat-treated HCT116 cells transfected with control or *p21* expression vectors and then treated with UC2288. (*G*) % Annexin V–FITC–positive cells was measured by FACS analysis of imetelstat-treated HCT116 cells transfected with control or *p21* expression vectors and then treated with UC2288. (*H*) Cleaved caspase 3 was measured by immunoblot in imetelstat-treated HCT116 cells transfected with control or *p21* expression vectors and then treated with UC2288. (*I*) Average tumor volumes of HCT116 xenograft from mice treated with vehicle, UC2288 alone, imetelstat alone, or both drugs. $^{**}P < 0.001$; $^{***}P < 0.0001$. (*J*) Average tumor volumes of ACHN xenograft from mice treated with vehicle, UC2288 alone, imetelstat alone, or both drugs. (*K*) Mouse-derived HCT116 xenograft tumors under indicated treatment conditions were analyzed for indicated proteins by immunoblot analysis. (*L*) Mouse-derived ACHN xenograft tumors under indicated treatment conditions were analyzed for indicated proteins by immunoblot analysis. $^{*}P < 0.01$; $^{**}P < 0.001$; $^{***}P < 0.0001$.

into the flanks of athymic nude mice and followed it by treatment with UC2288, imetelstat, or both drugs. Notably, combined treatment with UC2288 and imetelstat synergistically suppressed tumor growth (Fig. 6 *I–L* and *SI Appendix*, Table S2).

Toxicity analyses revealed that there were no significant differences in the body weight or ALT, AST, AP, whole blood counts, and renal activity markers in mice that were treated with imetelstat, UC2288, or both drugs, in comparison with the control group (*SI Appendix*, Fig. S15).

**Targeting Tumors Containing Mutant p53 Following Pharmacological Restoration of p53 Activity.** The results described above show that in the absence of p21, p53 and E2F1 cooperate to activate PUMA expression, which is necessary for apoptosis induction (Figs. 3 and 4). Accordingly, cells that lack functional p53 are less sensitive to imetelstat-mediated growth inhibition compared with cells containing wild-type p53 (Fig. 3*J*).

Approximately 50% of human cancers lack a functional p53 pathway, largely due to inactivating mutations in the p53 gene (41). We therefore asked whether simultaneous inhibition of telomerase and p21 could be adapted to treat cancers harboring p53 mutants. Previous studies have shown that the function of several different cancer-associated p53 mutants can be restored by treatment with small molecules such as CP-31398 (42, 43). CP-31398 alters the conformation of p53, thereby promoting its ability to bind to DNA (42, 43). As expected, treatment of p53 mutant cancer cell lines DLD1 (Ser241Phe), SW480 (Arg273His and Pro309Ser), and A375.S2 (Arg249Ser) with CP-31398 restored p53 activity, as evidenced by increased expression of its transcriptional target p21 (Fig. 7*A*). Next, using shRNAs, we knocked down *p21* in DLD1 and A375.S2 cells (Fig. 7*B*) and treated these cells with imetelstat and CP-31398. Treatment with both CP-31398 and imetelstat inhibited the growth of DLD1 and A375 cells expressing a *p21* shRNA more strongly compared with

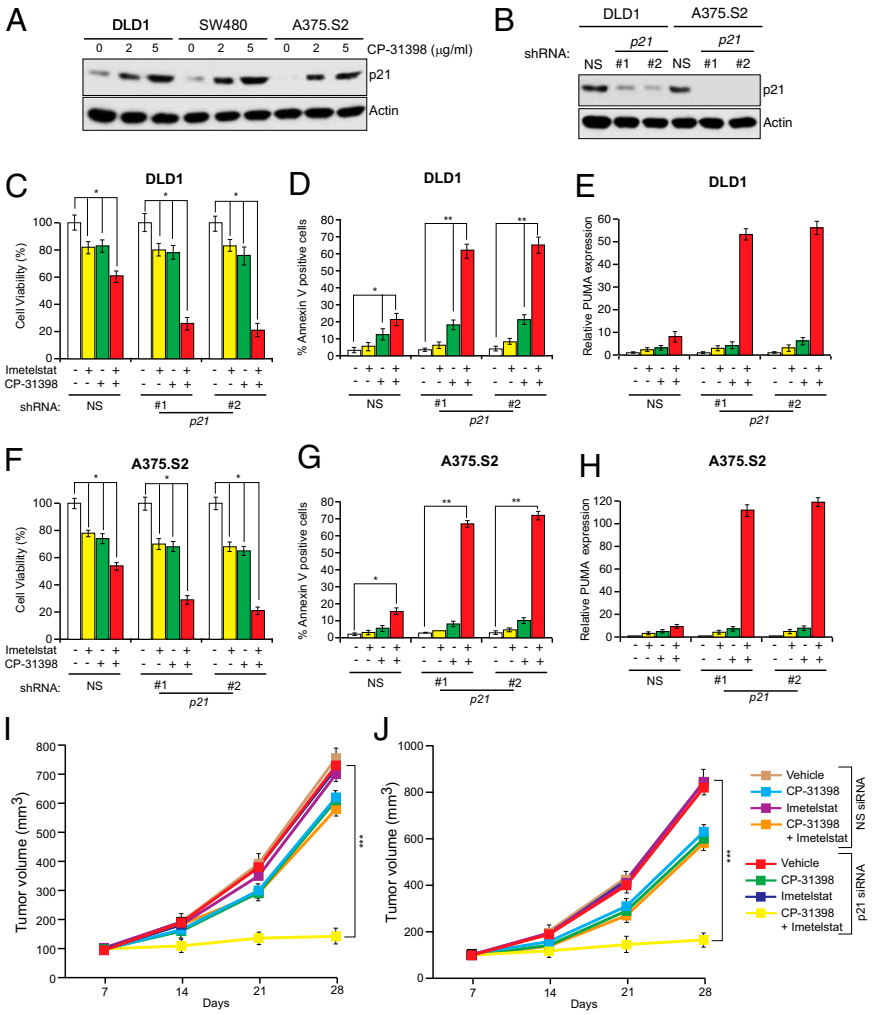


**Fig. 7.** Pharmacological restoration of p53 activity allows for the targeting of p53 mutant cancers by simultaneous p21 and telomerase inhibition. (*A*) Indicated p53 mutant cancer cell lines were treated at indicated concentrations of CP-31398 and analyzed for p21 expression by immunoblot. Actin was used as a loading control. (*B*) Indicated p53 mutant cancer cell lines expressing either an NS shRNA or shRNA targeting p21 were analyzed for p21 expression by immunoblot. Actin was used as a loading control. (*C* and *F*) DLD1 cells (*C*) or A375.S2 cells (*F*) expressing indicated shRNAs were treated with mismatch oligonucleotide or imetelstat for 6 wk and were either untreated or treated with CP-31398 for 2 d. Cell viability was measured by trypan blue assay, and relative cell viability is plotted. (*D* and *G*) DLD1 cells (*D*) or A375.S2 cells (*G*) expressing indicated shRNAs were treated with mismatch oligonucleotide or imetelstat for 6 wk and were either untreated or treated with CP-31398 for 2 d. Apoptosis was measured by Annexin V staining, and % apoptosis is plotted. (*E* and *H*) DLD1 cells (*E*) or A375.S2 cells (*H*) expressing indicated shRNAs were treated with mismatch oligonucleotide or imetelstat for 6 wk and were either untreated or treated with CP-31398 for 2 d. PUMA expression was measured by qRT-PCR. (*I* and *J*) Average tumor volumes of DLD1 xenograft (*I*) or A375.S2 (*J*) from mice treated with vehicle, CP-31398 alone, imetelstat alone, or both drugs with simultaneous treatment with nanoparticles with nonspecific or *p21* siRNA are shown. $*P < 0.01$; $**P < 0.001$; $***P < 0.0001$.

cells expressing a nonspecific shRNA (Fig. 7 *C* and *F* and *SI Appendix*, Fig. S16). Growth inhibition correlated with increased apoptosis (Fig. 7 *D* and *G*) and significantly higher PUMA activation (Fig. 7 *E* and *H*). Finally, we tested this approach for suppressing tumor growth in vivo. We found that addition of CP-31398 combined with simultaneous inhibition of telomerase and p21 substantially suppressed growth of tumors containing mutant p53 (Fig. 7 *I* and *J*). Collectively, these results show that simultaneous inhibition of telomerase and p21 can also be used to treat cancers containing mutant p53.

## Discussion

A large majority of diverse tumor types express telomerase, which is critical for cancer cell survival. Thus, inhibition of telomerase activity can block tumor cell growth both in vitro and in vivo. Due to such widespread expression and the requirement of telomerase for cancer cell survival, telomerase inhibitors can, in principle, be used to treat a broad spectrum of cancer types. In fact, telomerase inhibitors such as imetelstat have advanced into the clinic for the treatment of human cancers. However, for several reasons, single-agent telomerase therapies have not proven effective. First, because telomere shortening and consequential tumor growth inhibition require many cell divisions, single-agent telomerase inhibitors require substantial time to significantly decrease tumor growth. Second, telomerase inhibition typically results in only a cytostatic effect, which allows tumor cells to acquire secondary genetic and epigenetic alterations resulting in drug resistance. Finally, single-agent telomerase therapeutics often fail due to activation of ALT pathways, which bypasses the requirement for telomerase (25).

In this report, we have studied the role of p21 in telomerase inhibition-mediated growth suppression. We found that p21 loss increases apoptosis induction following telomerase inhibition in a variety of cancer cell lines and mouse xenografts. We further showed that apoptosis induction is specifically due to up-regulation of *PUMA* expression and that up-regulation of *PUMA* expression is dependent upon both p53 and E2F1. Although our results are consistent with other studies reporting that p21 can regulate apoptosis (9–13), the specific apoptotic mechanism we identify has not been previously described.

Previous studies have shown that p21 loss sensitizes cells to DNA-damage–induced apoptosis (9–13). In our experiments, treatment of cells with imetelstat induces a DNA damage response, which upon simultaneous loss of p21, results in apoptosis. Thus, the loss of p21 effectively converts the response of imetelstat from simple growth inhibition to apoptosis. According to this mechanism, the specificity of growth inhibition is due to imetelstat, which will selectively induce a DNA damage response in telomerase-positive cancer cells but not telomerase-negative normal cells.

Our finding that p21 is required to prevent apoptosis following telomerase inhibition reveals a critical genetic vulnerability of telomerase-expressing cancer cells. Accordingly, using both RNAi-based and pharmacological approaches, we showed that simultaneous inhibition of p21 and telomerase induces apoptosis in telomerase-positive human cancer cell lines and synergistically suppresses tumor growth. Specifically, we found that two unrelated pharmacological inhibitors of p21, sorafenib and UC2288, could function synergistically with imetelstat. Notably, in both cases, growth inhibition could be counteracted by ectopic expression of p21, indicating that sorafenib and UC2288 functioned by inhibiting p21 and not through an off-target effect. The induction of apoptosis by simultaneous inhibition of p21 and telomerase may greatly reduce the likelihood that resistance to telomerase inhibitors will develop through additional secondary genetic alterations or activation of ALT pathways. Finally, we show that simultaneous inhibition of telomerase and p21 also suppresses growth of tumors containing mutant p53 following pharmacological restoration of p53 activity.

Overall, we anticipate that simultaneous inhibition of telomerase and p21 can potentially overcome the current limitation of single-agent telomerase therapeutics and provide an effective method to treat a large number of cancers that rely on telomerase activity for survival, including the p53 mutant cancers.

## Materials and Methods

Materials and procedures for all experiments are supplied in *SI Appendix*. Included in *SI Appendix* are the mammalian cell culture procedures, details regarding tumorigenesis assay, protocols for TRAP assay to measure telomerase activity, Terminal Restriction Fragment analysis to measure telomere length, and ALT activity assay to monitor C-Circle amplification. Also provided are additional figures and tables providing p16 status of the cell lines used in our study, primer sequence information and antibody details used for immunolotting, and the statistical analyses of drug combinations to establish synergistic effects.

**ACKNOWLEDGMENTS.** We thank Bert Vogelstein, William G. Kaelin, and William Hahn for reagents. We thank Katia Bassett and Kevin Eng (Geron Corporation) for helpful discussions and Darryl Conte for editorial assistance. R.H.W. is supported by Grants 1R01CA135401-01A1 and 1R01DK082690-01A1 and B.D.H. is supported by Grant R01 ES002710. S.C. is supported by the Grant RO1 CA129037 from the National Cancer Institute. N.W. is a translational scholar of the Sidney Kimmel Foundation for Cancer Research and is supported by the Young Investigator grants from the National Lung Cancer Partnership, Uniting Against Lung Cancer Foundation, International Association for the Study of Lung Cancer, and Melanoma Research Alliance and Melanoma Research Foundation. M.R.G. is an investigator of the Howard Hughes Medical Institute.

1. Blackburn EH, Collins K (2011) Telomerase: An RNP enzyme synthesizes DNA. *Cold Spring Harb Perspect Biol* 3(5).
2. Shay JW, Wright WE (2011) Role of telomeres and telomerase in cancer. *Semin Cancer Biol* 21(6):349–353.
3. Hahn WC, et al. (1999) Inhibition of telomerase limits the growth of human cancer cells. *Nat Med* 5(10):1164–1170.
4. Chin L, et al. (1999) p53 deficiency rescues the adverse effects of telomere loss and cooperates with telomere dysfunction to accelerate carcinogenesis. *Cell* 97(4):527–538.
5. el-Deiry WS, et al. (1993) WAF1, a potential mediator of p53 tumor suppression. *Cell* 75(4):817–825.
6. Harper JW, Adami GR, Wei N, Keyomarsi K, Elledge SJ (1993) The p21 Cdk-interacting protein Cip1 is a potent inhibitor of G1 cyclin-dependent kinases. *Cell* 75(4):805–816.
7. Polyak K, Waldman T, He TC, Kinzler KW, Vogelstein B (1996) Genetic determinants of p53-induced apoptosis and growth arrest. *Genes Dev* 10(15):1945–1952.
8. Waldman T, Kinzler KW, Vogelstein B (1995) p21 is necessary for the p53-mediated G1 arrest in human cancer cells. *Cancer Res* 55(22):5187–5190.
9. Javelaud D, Besancon F (2002) Inactivation of p21WAF1 sensitizes cells to apoptosis via an increase of both p14ARF and p53 levels and an alteration of the Bax/Bcl-2 ratio. *J Biol Chem* 277(40):37949–37954.
10. Broude EV, et al. (2007) p21 (CDKN1A) is a negative regulator of p53 stability. *Cell Cycle* 6(12):1468–1471.
11. Xia M, Knezevic D, Vassilev LT (2011) p21 does not protect cancer cells from apoptosis induced by nongenotoxic p53 activation. *Oncogene* 30(3):346–355.
12. Dong C, Li Q, Lyu SC, Krensky AM, Clayberger C (2005) A novel apoptosis pathway activated by the carboxyl terminus of p21. *Blood* 105(3):1187–1194.
13. Chen Y, Zhang L, Jones KA (2011) SKIP counteracts p53-mediated apoptosis via selective regulation of p21Cip1 mRNA splicing. *Genes Dev* 25(7):701–716.
14. Röth A, Harley CB, Baerlocher GM (2010) Imetelstat (GRN163L)—Telomerase-based cancer therapy. *Recent Results Cancer Res* 184:221–234.
15. Macleod KF, et al. (1995) p53-dependent and independent expression of p21 during cell growth, differentiation, and DNA damage. *Genes Dev* 9(8):935–944.
16. Bunz F, et al. (1998) Requirement for p53 and p21 to sustain G2 arrest after DNA damage. *Science* 282(5393):1497–1501.
17. Goldberg M, et al. (2003) MDC1 is required for the intra-S-phase DNA damage checkpoint. *Nature* 421(6926):952–956.
18. Lou Z, Minter-Dykhouse K, Wu X, Chen J (2003) MDC1 is coupled to activated CHK2 in mammalian DNA damage response pathways. *Nature* 421(6926):957–961.
19. Stewart GS, Wang B, Bignell CR, Taylor AM, Elledge SJ (2003) MDC1 is a mediator of the mammalian DNA damage checkpoint. *Nature* 421(6926):961–966.
20. Dimitrova N, de Lange T (2006) MDC1 accelerates nonhomologous end-joining of dysfunctional telomeres. *Genes Dev* 20(23):3238–3243.
21. Zhu XD, Küster B, Mann M, Petrini JH, de Lange T (2000) Cell-cycle-regulated association of RAD50/MRE11/NBS1 with TRF2 and human telomeres. *Nat Genet* 25(3):347–352.
22. Kubo A, et al. (1999) The p16 status of tumor cell lines identifies small molecule inhibitors specific for cyclin-dependent kinase 4. *Clin Cancer Res* 5(12):4279–4286.

23. Lee EJ, et al. (2008) Histone deacetylase inhibitor scriptaid induces cell cycle arrest and epigenetic change in colon cancer cells. *Int J Oncol* 33(4):767–776.
24. Cesare AJ, Reddel RR (2010) Alternative lengthening of telomeres: Models, mechanisms and implications. *Nat Rev Genet* 11(5):319–330.
25. Hu J, et al. (2012) Antitelomerase therapy provokes ALT and mitochondrial adaptive mechanisms in cancer. *Cell* 148(4):651–663.
26. Henson JD, et al. (2009) DNA C-circles are specific and quantifiable markers of alternative-lengthening-of-telomeres activity. *Nat Biotechnol* 27(12):1181–1185.
27. Scheel C, et al. (2001) Alternative lengthening of telomeres is associated with chromosomal instability in osteosarcomas. *Oncogene* 20(29):3835–3844.
28. Miyashita T, Reed JC (1995) Tumor suppressor p53 is a direct transcriptional activator of the human bax gene. *Cell* 80(2):293–299.
29. Polyak K, Xia Y, Zweier JL, Kinzler KW, Vogelstein B (1997) A model for p53-induced apoptosis. *Nature* 389(6648):300–305.
30. Nakano K, Vousden KH (2001) PUMA, a novel proapoptotic gene, is induced by p53. *Mol Cell* 7(3):683–694.
31. Degenhardt K, Chen G, Lindsten T, White E (2002) BAX and BAK mediate p53-independent suppression of tumorigenesis. *Cancer Cell* 2(3):193–203.
32. Villunger A, et al. (2003) p53- and drug-induced apoptotic responses mediated by BH3-only proteins puma and noxa. *Science* 302(5647):1036–1038.
33. Carnevale J, Palander O, Seifried LA, Dick FA (2012) DNA damage signals through differentially modified E2F1 molecules to induce apoptosis. *Mol Cell Biol* 32(5):900–912.
34. Hershko T, Ginsberg D (2004) Up-regulation of Bcl-2 homology 3 (BH3)-only proteins by E2F1 mediates apoptosis. *J Biol Chem* 279(10):8627–8634.
35. Wang Y, Shen MF, Chang S (2011) Essential roles for Pot1b in HSC self-renewal and survival. *Blood* 118(23):6068–6077.
36. Woodrow KA, et al. (2009) Intravaginal gene silencing using biodegradable polymer nanoparticles densely loaded with small-interfering RNA. *Nat Mater* 8(6):526–533.
37. Cheng CJ, Saltzman WM (2011) Enhanced siRNA delivery into cells by exploiting the synergy between targeting ligands and cell-penetrating peptides. *Biomaterials* 32(26):6194–6203.
38. Inoue H, Hwang SH, Wecksler AT, Hammock BD, Weiss RH (2011) Sorafenib attenuates p21 in kidney cancer cells and augments cell death in combination with DNA-damaging chemotherapy. *Cancer Biol Ther* 12(9):827–836.
39. Wilhelm SM, et al. (2008) Preclinical overview of sorafenib, a multikinase inhibitor that targets both Raf and VEGF and PDGF receptor tyrosine kinase signaling. *Mol Cancer Ther* 7(10):3129–3140.
40. Wettersten HI, et al. (2013) A novel p21 attenuator which is structurally related to sorafenib. *Cancer Biol Ther* 14(3):278–285.
41. Brown CJ, Lain S, Verma CS, Fersht AR, Lane DP (2009) Awakening guardian angels: Drugging the p53 pathway. *Nat Rev Cancer* 9(12):862–873.
42. Foster BA, Coffey HA, Morin MJ, Rastinejad F (1999) Pharmacological rescue of mutant p53 conformation and function. *Science* 286(5449):2507–2510.
43. Takimoto R, et al. (2002) The mutant p53-conformation modifying drug, CP-31398, can induce apoptosis of human cancer cells and can stabilize wild-type p53 protein. *Cancer Biol Ther* 1(1):47–55.

**Supporting Information**

## Materials and Methods

### Cell culture

HCT116, p53KO, p21KO, and p21/PUMA DKO cells were a kind gift of Bert Vogelstein (Johns Hopkins Medical School). RKO, ACHN, LOX IMVI, UACC62, CAKI, NCI H460, DLD1, SW480, A375.S2 and U2OS cells were obtained from National Cancer Institute as part of the NCI 60 panel of cancer cell lines and from American Type Culture Collection (ATCC). The *p21* expression vector was a kind gift of William G. Kaelin (Dana Farber Cancer Institute). Cell lines were grown as recommended. *TERT* shRNAs were a kind gift of William Hahn (Harvard University). Lentiviral shRNA expression vectors were obtained from OpenBiosystems and were packaged by co-transfecting with lentiviral packaging plasmids into 293T cells using Effectene (Qiagen). After infection with lentivirus shRNA particles, cells stably transduced with lentiviral DNA were selected in medium containing puromycin. Cells were treated with 2.5 μM imetelstat or mismatch oligonucleotides (Geron Corporation) twice per week for up to 6 weeks and did not exceed 80% confluence during the treatment. Cells were treated with indicated concentrations of UC2288 at 80% confluence during the treatment. Cells were treated with indicated concentrations of CP-31398 at 80% confluence during the treatment.

### Cell viability and colony formation assay

For viability assays, cells were mixed with an equal volume of Trypan Blue Solution (Invitrogen) and counted using Countess (Invitrogen). For colony formation assays, $10^3$ cells were seeded in triplicate. Colonies were stained with 0.005% crystal-violet solution and counted after 10 days.

**Nanoparticle Synthesis**

PLGA nanoparticles loaded with siRNA were fabricated using a double emulsion solvent evaporation method and coated with ANTP as previously described (37). After washing unencapsulated siRNA and unattached ANTP, nanoparticles were lyophilized with the cryoprotectant, trehalose, at an equal mass ratio of polymer to carbohydrate.

**Tumorigenesis assays**

Eight-week old, athymic nude (NCr nu/nu) mice (n=5) were injected subcutaneously with cancer cells ($2.5x10^6$). After one week, tumor-bearing mice received mismatch oligonucleotide or imetelstat (30 mg/kg bodyweight) three times per week by intraperitoneal injection. Sorafenib was dissolved in Cremophor EL/95% ethanol (50:50) (Sigma) as a 4X stock solution and diluted with sterile water before use. Sorafenib (15 mg/kg) was administered by oral gavage three times per week. UC2888 was dissolved in Oleic acid with PEG400 as a 4X stock solution. UC2288 (15mg/kg body weight) was administered by oral gavage three times per week. For experiments using nanoparticles mice were injected with p21 or non-specific siRNA (1.0 mg/Kg body) two times a week. CP-31398 was administered at the concentration of 25 mg/kg everyday. Tumor growth was measured using calipers, and tumor volumes were calculated using the formula 0.5 X length X $width^2$. TUNEL assays were performed as described previously (1). For body weight measurements, mice were weighed at the end of the experiments before sacrifice. Blood was collected from the tail vein for alkaline aminotransferase (ALT), aspratate aminotransferase (AST) and alkaline phosophatase (AP) activity analysis. ALT, AST and AP activities were measured using kits from Sigma-Aldrich. For complete blood analyses we did the following

experiments: Hematocrit (Packed red cell volume) was analyzed and calculated as percentage of packed cell volume to the total volume. For RBC count 10 μl whole blood was diluted 1:1000 with PBS and RBC were counted using hemocytometer. For white blood cell count, we mixed 10 μl whole blood with RBC lysis reagent and after 1 minute of incubation the white cells were counted by hemocytometer. For measuring kidney function and as an indicator of glomerular filtration rate Serum creatinine levels were measured using Creatinine assay kit as per the manufacturers recommendations (Abcam).

**Quantitative RT-PCR analysis**

Total RNA was extracted with TRIzol (Invitrogen) and purified using RNAeasy mini columns (Qiagen). First-strand cDNA was generated using ProtoScript M-MuLV First-Strand cDNA Synthesis Kit (New England Biolabs), and quantitative PCR was performed using Power SYBR Green PCR Master Mix (Applied Biosystems). *p21*, *PUMA*, *BAX*, *BAK*, *TERT*, *MDC1, NBS1 CDKN1B (p27)* and *E2F1* expression were analyzed using primers listed in Table S3. *Actin* mRNA was measured as an internal control.

**Immunoblot analysis**

Cell lysates were prepared using Pierce IP Lysis Buffer (Thermo Scientific) containing Protease Inhibitor Cocktail (Roche) and Phosphatase Inhibitor Cocktail (Sigma-Aldrich, St. Louis, MO). Protein concentration was estimated using a Bradford Protein Assay kit (Bio-Rad Laboratories). Proteins were separated on 10% or 12% polyacrylamide gels and transferred to PVDF membranes using a Bio-Rad Trans-Blot wet transfer apparatus. Membranes were blocked with 5% nonfat milk and probed with primary antibodies followed by the appropriate secondary HRP-

conjugated antibody (GE healthcare, UK). Blots were developed using the SuperSignal West Pico Chemiluminescent Substrate (Pierce). Antibody information is provided in Table S3.

**FACS and Annexin V-FITC staining**

FACS analyses for sub G1 cell population were done as described previously (2). Briefly cells were fixed with 70% ethanol for overnight. The following day, cells were washed twice with 1X PBS and resuspended in 300 µl of 1X PBS, treated with RNAase (Sigma-Aldrich) and Propidium iodide for 1 hr and analyzed using FACSCaliber (BD Biosciences). Annexin V-FITC/PE staining were performed as described previously (3) using a kit available from BD Bioscience, stained cells were analyzed using FACSCaliber (BD Biosciences).

**TRAP assay**

The TRAP assay was performed essentially as described (4). Briefly, cells were washed once with ice cold PBS, resuspended in 100µL of ice-cold CHAPS lysis buffer (10 mM Tris-HCl (pH 7.5), 1 mM $MgCl_2$, 1 mM EGTA, 0.5% CHAPS, 10% glycerol and 5 mM beta-mercaptoethanol) and incubated 25 min on ice to lyse. Lysates were centrifuged for 20 min at 13,000 rpm at 4°C, supernatants were collected, and protein concentrations were measured using a Bradford Protein Assay Kit (Bio-Rad Laboratories). For the preparation of lysates equal weight tumor tissue was homogenized and processed similar to as described above. Telomerase activity was measured using a SYBR Green RQ-TRAP assay with 750 ng lysate, 0.1 µg telomerase primer TS and 0.05 µg anchored return primer ACX in a 25 µl reaction volume with SYBR Green PCR Master Mix (Applied Biosystems). TS and ACX primer sequences are provided in Table S3. Samples were analyzed using a CFX96 thermal cycler (Bio-Rad laboratories) by incubating for 20 minutes at

25°C, and amplified in a 35 cycle, two-step PCR with the conditions: 30 seconds at 95°C, and 90 seconds at 60°C. The threshold cycle values (Ct) were determined from semi-log amplification plots (log increase in fluorescence versus cycle number). Every plate included standards, inactivated samples and lysis buffer as controls. Each sample was analyzed at least in triplicate. Telomerase activity was plotted relative to untreated cells.

**Telomere PNA FISH analysis**

Peptide Nucleic Acid Fluorescence In Situ Hybridization (PNA FISH) was performed as described (5). Briefly, cells were treated with 0.5 μg/ml of colcemid for 3.5 hrs to arrest cells in metaphase. Trypsinized cells were incubated in 0.6 M KCl, fixed with methanol:acetic acid (3:1) and spread on glass slides. Metaphase chromosome spreads were hybridized with the telomeric PNA probe, 5′-Tam-OO-$(CCCTAA)_4$-3′. Chromosome images and telomere signals were captured and processed using a Nikon Eclipse 80i microscope and NIS-elements BR 3.1 software. At least 1000 chromosomes per sample were scored for telomere loss (i.e., signal free ends).

**Terminal Restriction Fragment (TRF) analysis**

Terminal Restriction Fragment (TRF) southern blot analysis was performed as described (6). Briefly, cells were trypsinized and embedded in 1% agarose plugs ($2x10^6$ cells per plug). Plugs were incubated in proteinase K digestion buffer (500 mM EDTA pH 8.0, 2% N- laurylsarcosine, and 20 mg/ml proteinase K) at 56ºC overnight. Plugs were washed with TE buffer for several hrs and then digested with RsaI and HinfI endonucleases at 37°C overnight. Plugs were loaded into 1% agarose gels for pulsed-field gel electrophoresis. After electrophoresis, gels were dried, and soaked in denaturing solution (0.2 N NaOH, 0.6 M NaCl) for 1 hr to denature DNA, followed by

neutralizing solution (1.5M NaCl, 0.5M Tris-Cl pH 7.4) for 1 hr. To detect telomere fragments, in-gel hybridization was performed using $\gamma$-$^{32}$P-$(CCCTAAA)_4$ oligonucleotide probe, gels were washed and exposed to a PhosphorImager screen. Telomere hybridization signals were scanned using a Typhoon PhosphorImager and quantified using ImageQuant software (GE).

**ALT activity assay by monitoring C-Circle amplification**

Rolling Circle Amplification (RCA) of C-circle DNA was performed as described (26), using $2x10^5$ cells per sample. The RCA reaction was carried out in 20µl reaction using 200 ng of DNA and from each samples ($1/10^{th}$) of the reaction was spotted to a Biodyne B membrane (Pall Corporation). Membranes were UV irradiated to crosslink DNA and pre-hybridized using PerfectHyb Plus hybridization buffer (Sigma-Aldrich) at 37°C for 1 hr. Membranes were hybridized with a $\gamma$-$^{32}$P-labelled $(CCCTAA)_3$ probe. The hybridized membrane was autoradiographed at -80°C for 1 day and developed to detect C-circle amplification products.

**Statistical Analysis**

All the experiments were performed at least three times in triplicates, and the data are expressed as Mean ± Standard Error Mean (SEM). Area Under the Curve (AUC) values were calculated using GraphPad Prism version 6.02 for Machintosh, GraphPad Software, San Diego California USA (www.graphpad.com). Student's t-test for two-tailed distribution with unequal variance was performed in Microsoft Excel to derive the p-values.

For synergy analyses, we used R, a system for statistical computation and graphics *(49)*, we assessed whether the combined effects from two drugs were additive (responses were equal to the sum of the single-drug effects), synergistic (greater than the sum of the single-drug effects)

or antagonistic (less than the sum of the single-drug effects) on tumor growth in a given cancer cell lines. Two-way analysis of variance (ANOVA) was used to test for the main effects of the drugs and their interaction on tumor size at the end point data for each all cell lines. Bonferroni correction was performed to counteract the problem of multiple comparisons (7). To determine whether various drug combinations exerted additive, synergistic or antagonistic impacts on decreasing tumor size, we compared the difference between observed effects with the expected additive effects for the mouse treated with both drugs (7). The difference was estimated as the interaction coefficient in the ANOVA. If there is a significant positive difference (i.e., interaction coefficient $> 0$ and Bonferroni adjusted p-value $< 0.01$), then the impact from the combined drugs was classified as antagonism. If there is a significant negative difference (i.e., interaction coefficient $< 0$ and Bonferroni adjusted p-value $< 0.01$), then the impact from the combined drugs was classified as synergistic on decreasing tumor size. If there is no significant difference, then the impact from the combined drugs was classified as additive.

**Supplementary Materials and Methods references**


1. Palakurthy RK, *et al.* (2009) Epigenetic silencing of the RASSF1A tumor suppressor gene through HOXB3-mediated induction of DNMT3B expression. (Translated from eng) *Mol Cell* 36(2):219-230 (in eng).
2. Santra MK, Wajapeyee N, & Green MR (2009) F-box protein FBXO31 mediates cyclin D1 degradation to induce G1 arrest after DNA damage. (Translated from eng) *Nature* 459(7247):722-725 (in eng).
3. Wajapeyee N, Serra RW, Zhu X, Mahalingam M, & Green MR (2008) Oncogenic BRAF induces senescence and apoptosis through pathways mediated by the secreted protein IGFBP7. (Translated from eng) *Cell* 132(3):363-374 (in eng).
4. Wege H, Chui MS, Le HT, Tran JM, & Zern MA (2003) SYBR Green real-time telomeric repeat amplification protocol for the rapid quantification of telomerase activity. (Translated from eng) *Nucleic Acids Res* 31(2):E3-3 (in eng).
5. Wu L, *et al.* (2006) Pot1 deficiency initiates DNA damage checkpoint activation and aberrant homologous recombination at telomeres. (Translated from eng) *Cell* 126(1):49-62 (in eng).
6. Blasco MA, *et al.* (1997) Telomere shortening and tumor formation by mouse cells lacking telomerase RNA. (Translated from eng) *Cell* 91(1):25-34 (in eng).
7. Slinker BK (1998) The statistics of synergism. (Translated from eng) *J Mol Cell Cardiol* 30(4):723-731 (in eng).

**Table S1. p16 status of the telomerase positive cancer cell lines used in this study.**

| Cell line | Alteration in p16 |
|---|---|
| ACHN | Homozygous deletion |
| CAKI | Homozygous deletion |
| HCT116 | Point mutation (Premature termination codon 80 (CGA-TGA) |
| LOX IMVI | Homozygous deletion |
| NCI H460 | Homozygous deletion |
| OVCAR5 | Homozygous deletion |
| RKO | DNA hypermethylation of the p16 promoter |
| UACC62 | Homozygous deletion |

**Table S2. Results of statistical analyses to determine synergism, antagonism and additive effects among indicated siRNA and drug combinations.**

| Cell line | Effect | Coefficient | p-Value | Synergism/Antagonism/Additive | Bonferroni Adjusted p-value |
|---|---|---|---|---|---|
| **HCT116** | Nanoparticle encapsulated p21 siRNA main effect | 103.4 | .00144248 | | 1.88E-02 |
| | Imetelstat main effect | -118.6 | 9.4-E-08 | | 1.22E-06 |
| | **p21 siRNA: Imetelstat interaction** | **-528.4** | **1.04E-05** | **Synergism** | **1.35E-04** |
| **ACHN** | Nanoparticle encapsulated p21 siRNA main effect | 44 | 3.75E-22 | | 4.88E-21 |
| | Imetelstat main effect | -89 | 4.94E-26 | | 6.24E-25 |
| | **p21 siRNA: Imetelstat interaction** | **-443** | **1.09E-23** | **Synergism** | **1.42E-22** |
| **HCT116** | Sorafenib main effect | -182 | 2.43E-22 | | 3.159E-21 |
| | Imetelstat main effect | -241 | 5.30E-24 | | 6.89E-23 |
| | **Sorafenib: Imetelstat interaction** | **-72** | **4.23E-10** | **Synergism** | **5.499E-20** |
| **RKO** | Sorafenib main effect | -173 | 1.34E-33 | | 1.742E-21 |
| | Imetelstat main effect | -131 | 2.78E-21 | | 3.614E-20 |
| | **Sorafenib: Imetelstat interaction** | **-139** | **5.35E-14** | **Synergism** | **6.955E-13** |
| **ACHN** | Sorafenib main effect | -120 | 8.49E-20 | | 1.1037E-18 |
| | Imetelstat main effect | -70 | 5.71E-18 | | 7.423E-17 |
| | **Sorafenib: Imetelstat interaction** | **-190** | **3.44E-14** | **Synergism** | **4.472E-13** |
| **LOXIMVI** | Sorafenib main effect | -80 | 2.17E-20 | | 2.82E-19 |
| | Imetelstat main effect | -202 | 9.92E-24 | | 1.29E-22 |
| | **Sorafenib: Imetelstat interaction** | **-234** | **8.54E-17** | **Synergism** | **1.11E-15** |
| **UACC62** | Sorafenib main effect | -42 | 4.98E-19 | | 6.47E-18 |
| | Imetelstat main effect | -294 | 4.06E-25 | | 5.28E-24 |
| | **Sorafenib: Imetelstat interaction** | **-274** | **3.47E-17** | **Synergism** | **4.51E-16** |
| **CAKI** | Sorafenib main effect | -30 | 2.70E-20 | | 3.15E-19 |
| | Imetelstat main effect | -205 | 3.74E-25 | | 4.86E-24 |
| | **Sorafenib: Imetelstat interaction** | **-265** | **1.12E-18** | **Synergism** | **1.46E-17** |
| **HCT116** | UC2288 main effect | -90 | 1.18E-19 | | 1.53E-18 |
| | Imetelstat main effect | -295 | 3.57E-24 | | 4.641E-23 |
| | **UC2288: Imetelstat interaction** | **-266** | **4.27E-16** | **Synergism** | **5.55E-15** |
| **ACHN** | UC2288 main effect | -18 | 1.01E-19 | | 1.313E-18 |
| | Imetelstat main effect | -128 | 7.56E-23 | | 9.828E-22 |
| | **UC2288:Imetelstat interaction** | **-350** | **4.78E-19** | **Synergism** | **6.214E-18** |

**Table S3. Primer sequences for RT-qPCR analysis; clone ID and catalog numbers for shRNAs (Open Biosystems); antibodies used; source and concentration of chemical inhibitors used.**

| Application | Gene symbol | Forward primer (5′-3′) | Reverse primer (5′-3′) |
|---|---|---|---|
| RT-qPCR | *CDKN1A (p21)* | GCAGACCAGCATGACAGATTT | GGATTAGGGCTTCCTCTTGGA |
| | *PUMA* | TCGGTGCTCCTTCACTCTGG | GCAAACGAGCCCCACTCTCT |
| | *BAX* | ACCAAGGTGCCGGAACTGAT | ACTCCCGCCACAAAGATGGT |
| | *BAK* | GCCCAGGACACAGAGGAGGT | CCATGGTGCTGCTAGGTTGC |
| | *ACTIN* | GCATGGAGTCCTGTGGCATC | TTCTGCATCCTGTCGGCAAT |
| | *E2F1* | TCCCTCCTGCAGTGTCTGAA | CAGCGAGGAAGCTGACCTTT |
| | *MDC1* | GCCTTTTGACACGCACCTTG | GCCCACCCTCTCTGCTGTTT |
| | *NBS1* | TGTCAGGACGGCAGGAAAGA | TTCCCGGAGCAAAAAGAAA |
| | *CDKN1B (p27)* | GCTCCGGCTAACTCTGAGGA | AAGAATCGTCGGTTGCAGGT |
| | *TERT* | GACACACATTCCACAGGTCG | GACTCGACACCGTGTCACCTAC |
| | *ACX* | GCGCGGCTTACCCTTACCCTTACCCTAACC | |
| | *TS* | AATCCGTCGAGCAGAGTT | |
| | *RCA* | CCCTAACCCTAACCCTAA | |
| | | | |
| | **Gene symbol** | **Clone ID** | **Catalog number** |
| shRNAs | *CDKN1A (p21)* | TRCN0000040123 | RHS3979-9607512 |
| | | TRCN0000040125 | RHS3979-9607514 |
| | *MDC1* | TRCN0000018850 | RHS3979-9586172 |
| | | TRCN0000018851 | RHS3979-9586173 |
| | *NBS1* | TRCN0000040137 | RHS3979-9607526 |
| | | TRCN0000010393 | RHS3979-9630894 |
| | *E2F1* | TRCN0000000251 | RHS3979-9568611 |
| | | TRCN0000000253 | RHS3979-9568613 |
| | *PUMA* | TRCN0000033611 | RHS3979-9601019 |
| | CDKN1B | TRCN0000039929 | RHS3979-9607318 |
| | | TRCN0000009856 | RHS3979-97079654 |
| siRNA | **Gene symbol** | | **Sequence** |
| | CDKN1A (p21) | Thermoscientific | GCGAUGGAACUUCGACUUU |
| | Non-targeting | Thermoscientific | UAAGGCUAUGAAGAGAUAC |
| | | | |
| | **Protein symbol** | **Antibody source** | |
| Immunoblot/ | CDKN1A (p21) | Santa Cruz Biotechnology, Inc. | |
| ChIP | PUMA | Thermo Scientific | |
| | BAX | Santa Cruz Biotechnology, Inc. | |
| | BAK | Santa Cruz Biotechnology, Inc. | |
| | TERT | R & D Systems | |
| | p53 | Santa Cruz Biotechnology, Inc. | |
| | Cleaved caspase 3 | Cell signaling | |
| | Actin | Sigma-Aldrich | |
| | | | |
| | **Inhibitor** | **Concentration** | **Source** |
| | Imetelstat | 2.5 μM | Geron Corporation |
| | Mismatch Oligonucleotide | 2.5 μM | Geron Corporation |

| | | | |
|---|---|---|---|
| | Sorafenib | 1 μM and 2.5 μM | LC Laboratories |
| | UC2288 | 1 μM, 2.5 μM and 5 μM | |
| | CP-31398 | 2 and 5 μg/ml | Sigma-Aldrich |

**Supplementary figure legends**

**Fig. S1. shRNA-mediated inhibition of *TERT* expression leads to potent growth inhibition in HCT116 p21KO cells.** Analysis of HCT116 p21KO (*A–D*) or wild-type (*E–H*) cells stably transduced with non-specific control (NS) or two different *TERT* shRNAs. (*A, E*) qRT-PCR analysis of *TERT* mRNA. (*B, F*) Cell viability as measured by trypan blue exclusion assay. Cell viability relative to non-specific shRNA is plotted. (*C, G*) Annexin V-FITC positive cells were quantified by FACS analysis. % Annexin V-FITC positive cells are plotted. (*D, H*) Telomerase activity as measured by the TRAP assay and plotted relative to the mismatch oligonucleotide. *** represents $p<0.0001$.

**Fig. S2. shRNA-mediated loss of *p21* leads to apoptosis induction upon telomerase inhibition.** Analysis of HCT116 cells stably transduced with non-specific control (NS) or two different *p21* shRNAs. (*A*) Immunoblot analysis of p21 protein. (*B*) qRT-PCR analysis of *p21* mRNA. (*C-F*) Cells were treated with mismatch oligonucleotide or with imetelstat for 6 weeks. (*C*) Colony formation monitored by crystal violet staining. (*D*) Cell viability as measured by trypan blue exclusion assay. Cell viability relative to mismatch oligonucleotide is plotted. (*E*) Apoptosis monitored by FACS analysis. (*F*) Annexin V-FITC positive cells were quantified using FACS analysis. % Annexin V-FITC positive cells are plotted. (*G*) Telomerase activity as measured by the TRAP assay and plotted relative to the mismatch oligonucleotide. ** and *** represents $p<0.001$ and $p<0.0001$ respectively.

**Fig. S3. shRNA-mediated *p21* knockdown in unrelated human cancer cell lines sensitize them to telomerase inhibition-mediated apoptosis.** (*A, B*) Immunoblot analysis of RKO (*A*) and ACHN (*B*) cells stably transduced with non-specific control (NS) or two different *p21* shRNAs. (*C*) (Left) *p21* gene specific probes intensity values for the indicated cell lines were obtained from BioGPS, Relative *p21* expression is plotted. (Right) Immunoblot analysis to monitor p21 expression levels in the indicated cell lines. Actin was used as a loading control. (*D-F*) Indicated cells were treated with mismatch oligonucleotide or with imetelstat for 6 weeks. (*D*) Cell viability was measured by trypan blue exclusion assay. Cell viability relative to mismatch oligonucleotide is plotted. (*E*) Annexin V-FITC positive cells were quantified for indicated cell lines using FACS analyses. % Annexin V positive cells under indicated conditions is plotted. (*F*) Telomerase activity as measured by the TRAP assay and plotted relative to the mismatch oligonucleotide. (*G*) Dot blot analysis of rolling circle amplification of C-circle DNA to measure ALT activity in the indicated cell lines. ** and *** represents $p<0.001$ and $p<0.0001$ respectively.

**Fig. S4. Loss of checkpoint proteins MDC1 or NBS1 do not cooperate with telomerase inhibition to induce growth arrest.** HCT116 cells stably transduced with *MDC1* (*A–F*) or *NBS1* (*G–L*) shRNAs. Where indicated, cells were treated either with mismatch oligonucleotide or imetelstat for 6 weeks. (*A, G*) qRT-PCR analysis of *MDC1* (*A*) or *NBS1* (*G*) mRNA. (*B, H*) Colony formation monitored by crystal violet staining. (*C, I*) Cell viability as measured by trypan blue exclusion assay. Cell viability relative to mismatch oligonucleotide is plotted. (*D, J*) Apoptosis monitored by FACS analysis. (*E, K*) Telomerase activity as measured by the TRAP

assay and plotted relative to the mismatch oligonucleotide. (*F, L*) qRT-PCR analysis of *PUMA* mRNA. *** represents $p<0.0001$.

**Fig. S5. Loss of cyclin dependent kinase inhibitor p27 does not cooperate with telomerase inhibition to induce growth arrest.** HCT116 cells stably transduced with *p27* shRNAs and where indicated, cells were treated either with mismatch oligonucleotide or imetelstat for 6 weeks. (*A*) qRT-PCR analysis of *p27* mRNA. (*B*) Colony formation monitored by crystal violet staining. (*C*) Cell viability as measured by trypan blue exclusion assay. Cell viability relative to mismatch oligonucleotide is plotted. (*D*) Apoptosis monitored by FACS analysis of sub G1 population. (*E*) Telomerase activity as measured by the TRAP assay and plotted relative to the mismatch oligonucleotide. (*F*) qRT-PCR analysis of *PUMA* mRNA.

**Fig. S6. ER-stress inducer tunicamycin does not enhance tumor cell growth after Imetelstat treatment or loss of p21.** (*A*) Relative cell viability measured by trypan blue exclusion assay of HCT116 cells that were either remained untreated or treated with imetelstat, tunicamycin or both. (*B*) Apoptosis was measured by Annexin V-FITC staining for HCT116 cells that were either remained untreated or treated with imetelstat, tunicamycin or both. (*C*) Relative cell viability measured by trypan blue exclusion assay of HCT116 wild type or p21 KO cells that were either remained untreated or treated with tunicamycin. (*D*) Apoptosis was measured by Annexin V-FITC staining for HCT116 wild type or p21 KO cells that were either remained untreated or treated with tunicamycin.

**Fig. S7. *p21* does not regulate the ability of imetelstat to inhibit telomerase activity, telomere shortening or ALT.** Indicated cell lines were treated with mismatch oligonucleotide or imetelstat for 6 weeks. (*A*) Southern blot to measure telomere length. Size markers in kilobase are shown next to the gel image. (*B*) Telomere length relative to HCT116 cells treated with mismatch oligonucleotide, in all indicated cell lines corresponding to (*A*) is presented. (*C*) Telomere PNA-FISH to monitor signal-free chromosomal ends. (*D*) Signal-free chromosomal ends in (*C*) were quantified and plotted relative to mismatch oligonucleotide. (*E*) Dot blot analysis of rolling circle amplification of C-circle DNA to measure ALT activity in the indicated cell lines. ** represents $p<0.001$.

**Fig. S8. Treatment of ALT activated cell line U2OS with imetelstat did not induce growth inhibition irrespective of p21 expression.** (*A, B*) U2OS cells expressing indicated shRNAs were treated with either a mismatch oligonucleotide or with Imetelstat for 6 weeks. (*A*) Colony formation was monitored by crystal violet staining. (*B*) cell viability was measured by trypan blue exclusion assay

**Fig. S9. *PUMA* activation is a general requirement for telomerase inhibition-induced tumor suppression.** (*A, B*) RKO cells with indicated shRNAs were treated with either a mismatch oligonucleotide or imetelstat for 6 weeks. (*A*) Fold change in *PUMA* transcript levels measured by qRT-PCR (*B*) Immunoblot analysis was performed for indicated proteins. (*C*) *PUMA* knockdown in *p21* shRNA expressing RKO cells was confirmed by qRT-PCR. (*D-F*) RKO cells with indicated shRNAs were treated with either a mismatch oligonucleotide or imetelstat for 6 weeks. (*D*) Relative cell viability was measured by trypan blue exclusion assay.

(*E*) Annexin V-FITC positive cells were quantified using FACS analysis. % Annexin V-FITC positive cells are plotted. (*F*) Relative telomerase activities of indicated cells. (*G, H*) ACHN cells with indicated shRNAs were treated with either a mismatch oligonucleotide or imetelstat for 6 weeks. (*G*) Fold change in *PUMA* transcript levels measured by qRT-PCR. (*H*) Immunoblot analysis was performed for indicated proteins. *(I*) *PUMA* knockdown in *p21* shRNA expressing ACHN cells was confirmed by qRT-PCR. (*J-L*) ACHN cells with indicated shRNAs were treated with either a mismatch oligonucleotide or imetelstat for 6 weeks. (*J*) Cell viability was measured by trypan blue exclusion assay. (*K*) Annexin V-FITC positive cells were quantified using FACS analysis. % Annexin V-FITC positive cells are plotted. (*L*) Relative telomerase activities of indicated cells. ** represents $p<0.001$.

**Fig. S10. Analyses of telomerase activity by TRAP assay.** (*A*) Relative telomerase activities of HCT116 p21KO cells expressing indicated shRNAs and treated with a mismatch oligonucleotide (-) or with imetelstat (+). (*B*) Relative telomerase activities of HCT116 wild type and p53KO cells treated with a mismatch oligonucleotide (-) or with imetelstat (+).

**Fig. S11. Telomerase inhibition-induces strong tumor suppression in cancer cells with lower *p21* expression in a *PUMA* dependent manner.** (*A*) Indicated cell lines were treated with either a mismatch oligonucleotide or imetelstat for 6 weeks. Fold change in *PUMA* transcript levels measured by qRT-PCR. (*B*) *PUMA* knockdown in NCI H460 and OVCAR5 cells was confirmed by qRT-PCR. (*C, D*) Indicated cell lines were treated with either a mismatch oligonucleotide or imetelstat. (*C*) Cell viability was measured by trypan blue exclusion assay.

(*D*) Relative telomerase activities of indicated cells. * and ** represents $p<0.01$ and $p<0.001$ respectively.

**Fig. S12. Nanoparticle-based systemic p21 siRNA delivery inhibits the growth of tumors in combination with imetelstat treatment.** (*A*) HCT116 cells were injected into the flanks of nude mice and were treated as indicated. Tumor volumes at indicated days are shown and the representative tumors are presented. (*B*) ACHN cells were injected into the flanks of nude mice and were treated as indicated. Tumor volumes at indicated days are shown and the representative tumors are presented. (*C*) Mouse derived HCT116 xenograft tumor under indicated treatment conditions were analyzed for indicated proteins by immunoblot analysis. (*D*) Mouse derived ACHN xenograft tumor under indicated treatment conditions were analyzed for indicated proteins by immunoblot analysis. (*E*) Mouse derived HCT116 xenograft tumor under indicated treatment conditions were analyzed for telomerase activity by TRAP assay. (*F*) Mouse derived ACHN xenograft tumor under indicated treatment conditions were analyzed for telomerase activity by TRAP assay. * , **, *** represents $p<0.01$, $p<0.001$, $p<0.0001$ respectively

**Fig. S13. Analyses of the drug toxicity of sorafinib, imetelstat and their combination in mice.** (*A*) Control mice group bearing HCT116 tumors or HCT116 tumor bearing mice treated with the indicated drugs were weighed at the end of the experiment. Average reduction in body weight in drug treatment group is plotted in comparison to control mice. (*B*) Activities of alanine aminotransferase (ALT), aspartate aminotransferase (AST) and alkaline phosphatase (AP) were analyzed in the sera of the indicated mice groups. Activities of these enzymes in comparison to the control mice group is plotted. (*C*) Relative hemacrite (packed red cell volume) level in

HCT116 tumor bearing mice, compared to vehicle control. (*D*) Relative Red Blood cell (RBC) count in HCT116 tumor bearing mice under indicated condition, compared to vehicle control. (*E*) Relative White blood cell (WBC) count in HCT116 tumor bearing mice under indicated condition, compared to vehicle control. (*F*) Activity of creatinine in the sera of the indicated mice groups. Activities in comparison to the control mice group is plotted.

**Fig. S14. Simultaneous inhibition of telomerase and p21 cause synergistic tumor suppression in a wide variety of cancer cells.** (*A*-*E*) Average tumor volumes from mice treated with vehicle, sorafenib alone, imetelstat alone or with both drugs for indicated cell lines. *** represents $p<0.0001$.

**Fig. S15. Analyses of the drug toxicity of UC2288, imetelstat and their combination in mice.** (*A*) Control mice group bearing HCT116 tumors or HCT116 tumor bearing mice treated with the indicated drugs were weighed at the end of the experiment. Average reduction in body weight in drug treatment group is plotted in comparison to control mice. (*B*) Activities of alanine aminotransferase (ALT), aspartate aminotransferase (AST) and alkaline phosphatase (AP) were analyzed in the sera of the indicated mice groups. Activities of these enzymes in comparison to the control mice group is plotted. (*C*) Relative hemacrite (packed red cell volume) level in HCT116 tumor bearing mice, compared to vehicle control. (*D*) Relative Red Blood cell (RBC) count in HCT116 tumor bearing mice under indicated condition, compared to vehicle control. (*E*) Relative White blood cell (WBC) count in HCT116 tumor bearing mice under indicated condition, compared to vehicle control. (*F*) Activity of creatinine in the sera of the indicated mice groups. Activities in comparison to the control mice group, is plotted.

**Fig. S16. Telomerase activity measurement**. DLD1 (**Left**) and A375.S2 (**Right**) cells treated as indicated were analyzed for telomerase activity. Relative telomerase activity is plotted.

**Fig. S1**

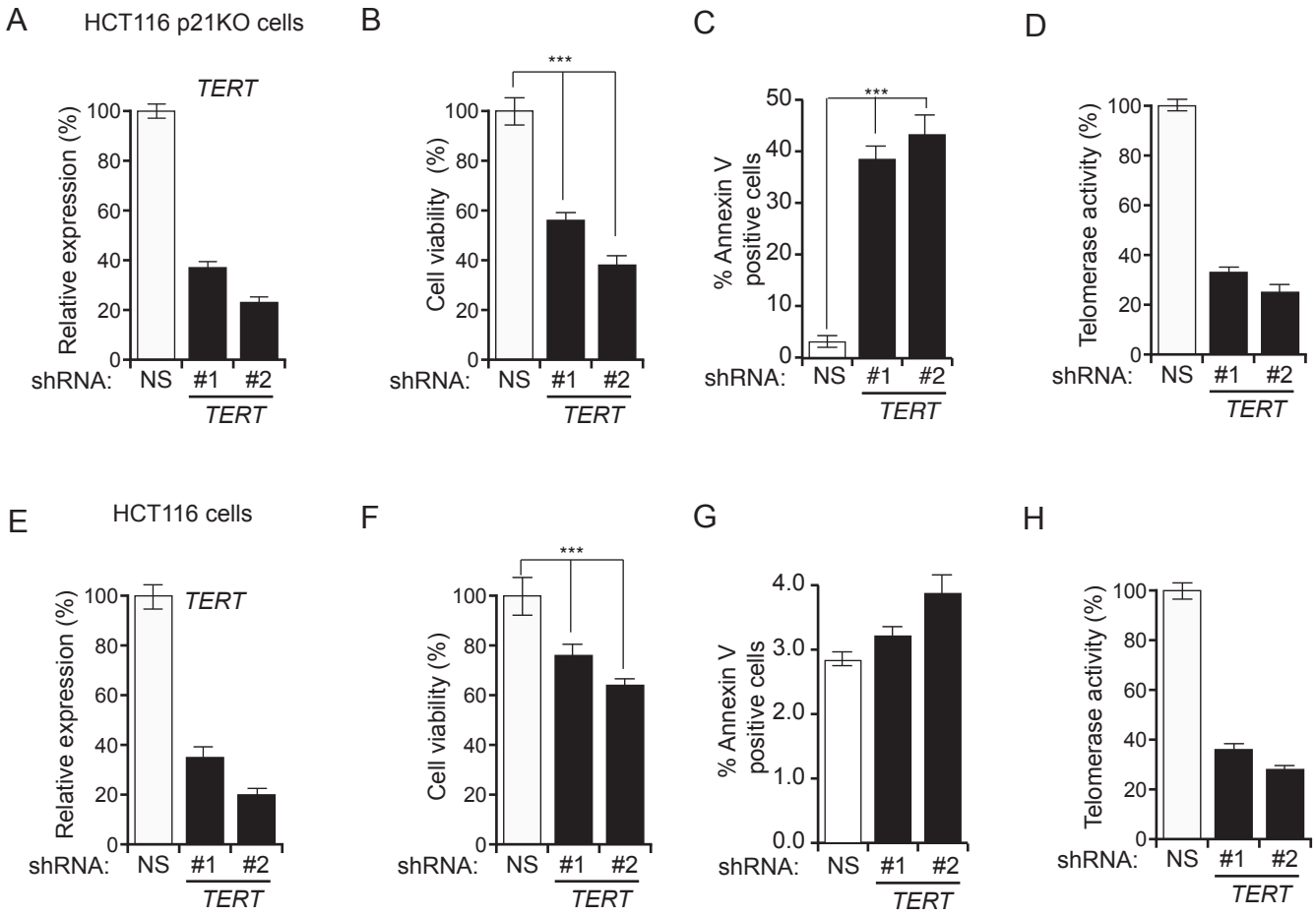
A
HCT116 p21KO cells
TERT
Relative expression (%)
100
80
60
40
20
0
shRNA:
NS
#1
#2
TERT
B
***
Cell viability (%)
C
% Annexin V positive cells
50
40
30
20
10
0
D
Telomerase activity (%)
E
HCT116 cells
F
G
4.0
3.0
2.0
1.0
0.0
H

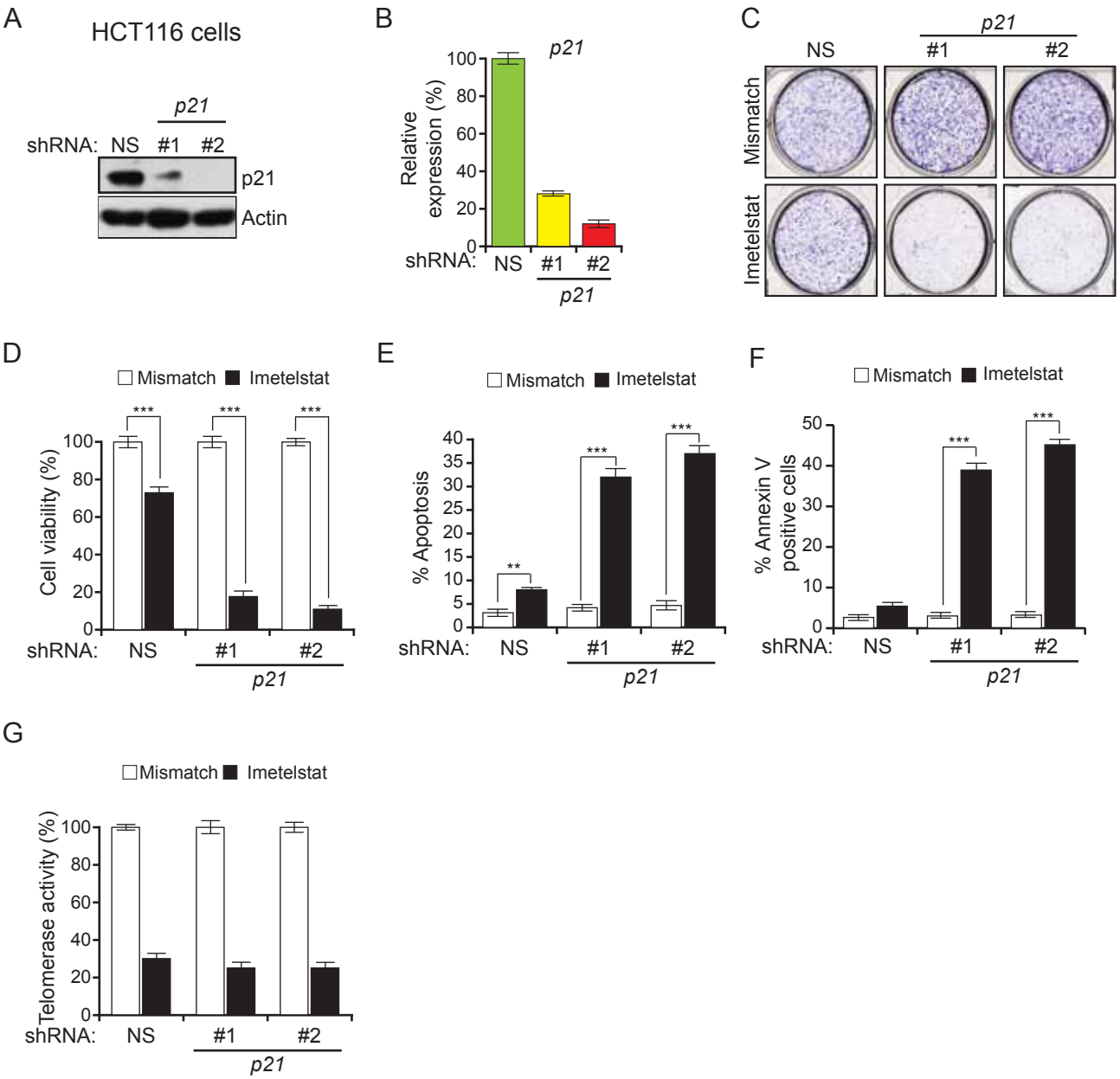
A
HCT116 cells
p21
shRNA: NS #1 #2
p21
Actin
B
p21
Relative expression (%)
100
80
60
40
20
0
shRNA: NS #1 #2
p21
C
p21
NS #1 #2
Mismatch
Imetelstat
D
Mismatch Imetelstat
Cell viability (%)
***
shRNA: NS #1 #2
p21
E
Mismatch Imetelstat
% Apoptosis
**
***
shRNA: NS #1 #2
p21
F
Mismatch Imetelstat
% Annexin V positive cells
***
shRNA: NS #1 #2
p21
G
Mismatch Imetelstat
Telomerase activity (%)
shRNA: NS #1 #2
p21

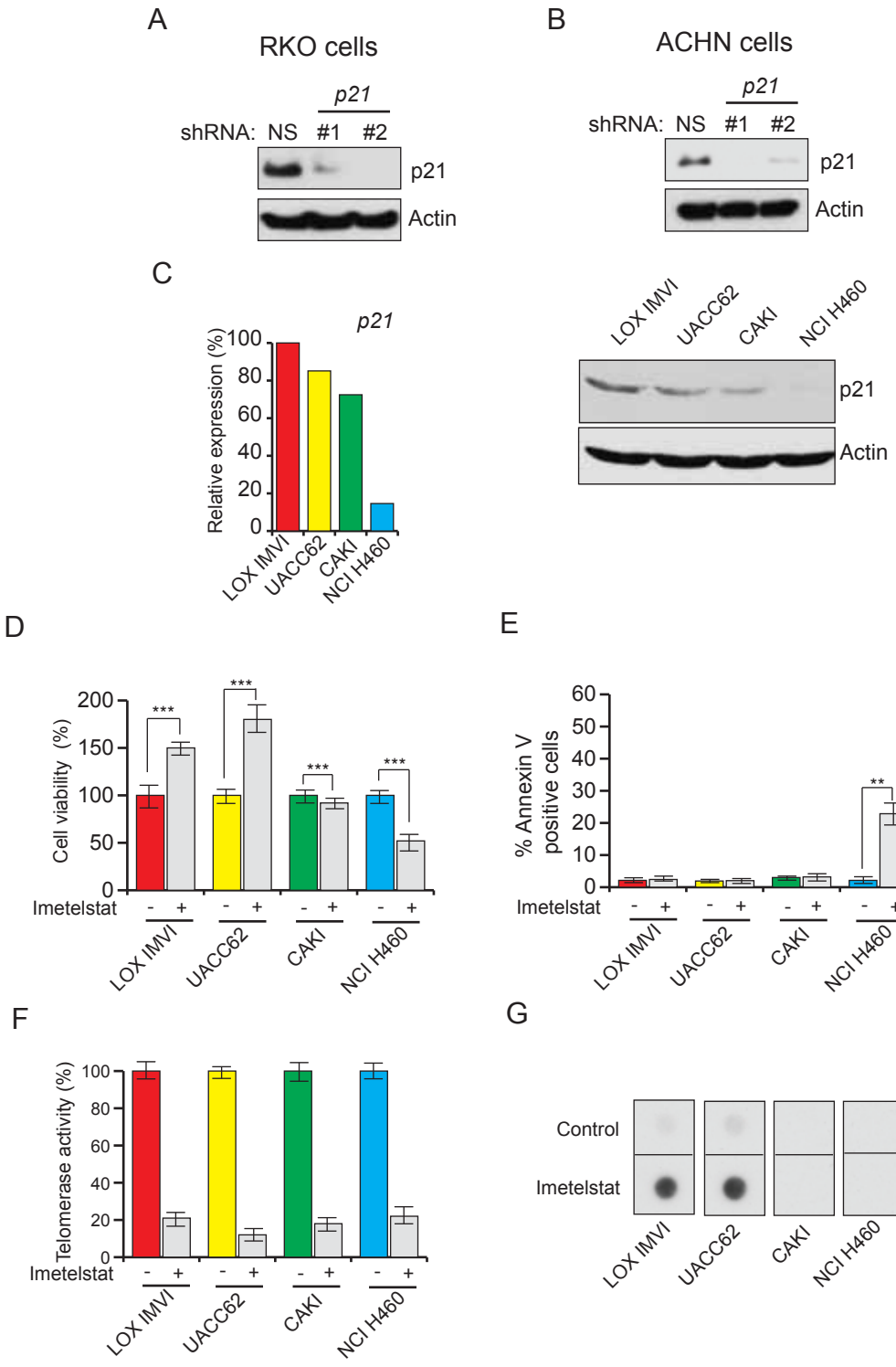
A
RKO cells
p21
shRNA: NS #1 #2
p21
Actin
B
ACHN cells
p21
shRNA: NS #1 #2
p21
Actin
C
p21
Relative expression (%)
100
80
60
40
20
0
LOX IMVI
UACC62
CAKI
NCI H460
LOX IMVI
UACC62
CAKI
NCI H460
p21
Actin
D
Cell viability (%)
200
150
100
50
0
***
***
***
***
Imetelstat
- + - + - + - +
LOX IMVI
UACC62
CAKI
NCI H460
E
% Annexin V positive cells
60
50
40
30
20
10
0
**
Imetelstat
- + - + - + - +
LOX IMVI
UACC62
CAKI
NCI H460
F
Telomerase activity (%)
100
80
60
40
20
0
Imetelstat
- + - + - + - +
LOX IMVI
UACC62
CAKI
NCI H460
G
Control
Imetelstat
LOX IMVI
UACC62
CAKI
NCI H460

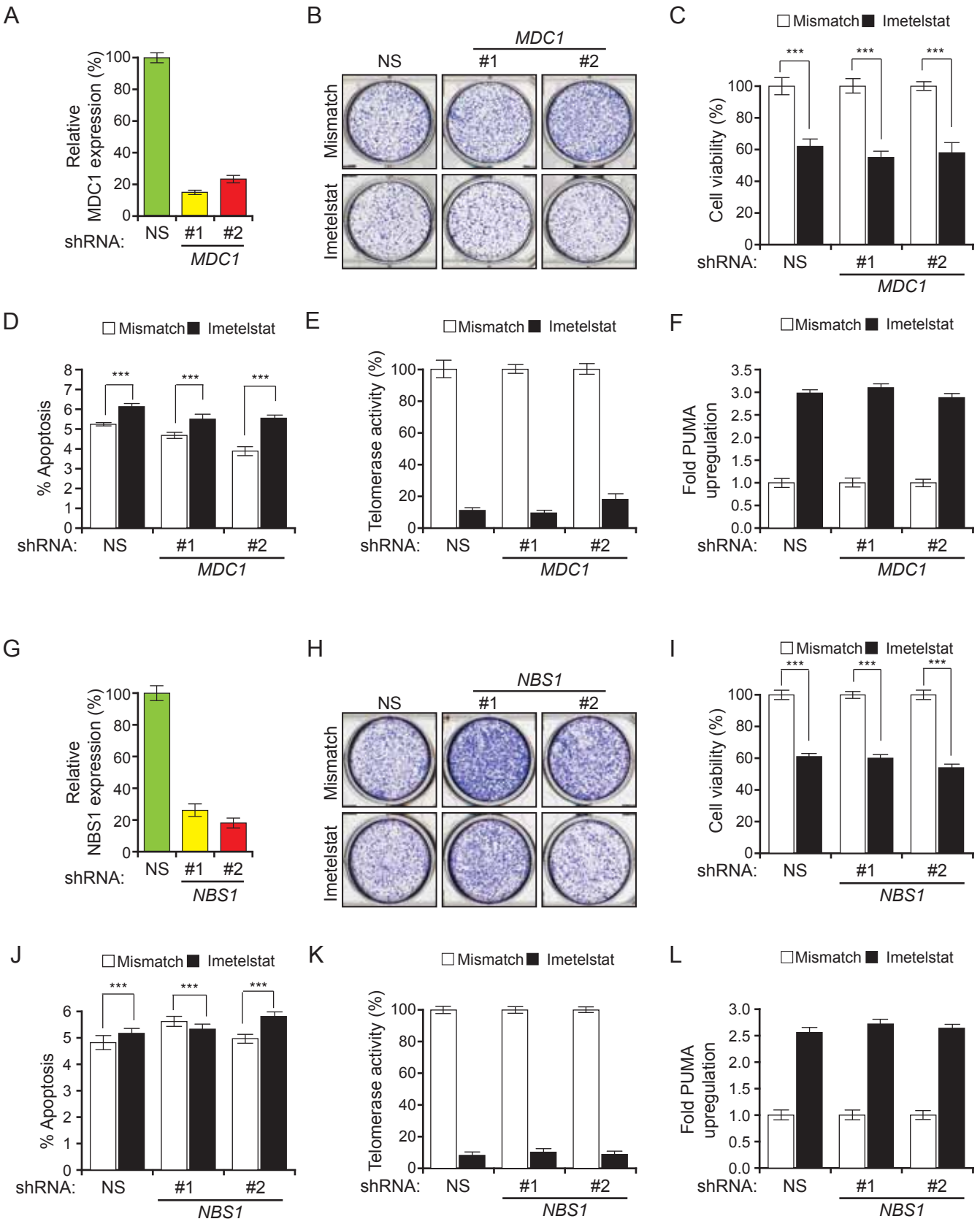
A
Relative MDC1 expression (%)
100
80
60
40
20
0
shRNA:
NS
#1
#2
MDC1
B
MDC1
NS
#1
#2
Mismatch
Imetelstat
C
Mismatch
Imetelstat
***
Cell viability (%)
shRNA:
NS
#1
#2
MDC1
D
Mismatch
Imetelstat
% Apoptosis
8
7
6
5
4
3
2
1
0
***
shRNA:
NS
#1
#2
MDC1
E
Mismatch
Imetelstat
Telomerase activity (%)
shRNA:
NS
#1
#2
MDC1
F
Mismatch
Imetelstat
Fold PUMA upregulation
3.5
3.0
2.5
2.0
1.5
1.0
0.5
0.0
shRNA:
NS
#1
#2
MDC1
G
Relative NBS1 expression (%)
shRNA:
NS
#1
#2
NBS1
H
NBS1
NS
#1
#2
Mismatch
Imetelstat
I
Mismatch
Imetelstat
Cell viability (%)
shRNA:
NS
#1
#2
NBS1
J
Mismatch
Imetelstat
% Apoptosis
shRNA:
NS
#1
#2
NBS1
K
Mismatch
Imetelstat
Telomerase activity (%)
shRNA:
NS
#1
#2
NBS1
L
Mismatch
Imetelstat
Fold PUMA upregulation
shRNA:
NS
#1
#2
NBS1

**Fig. S5**

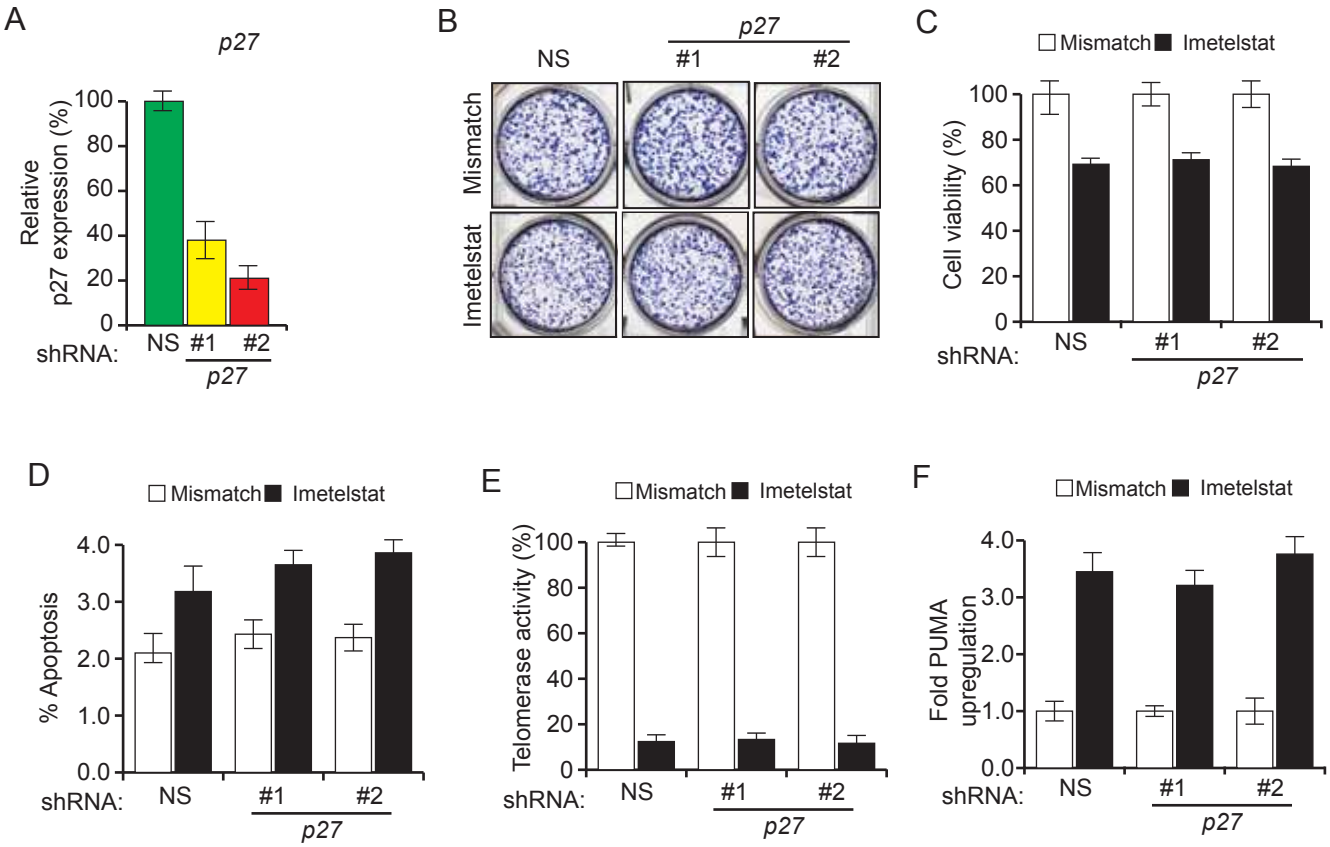
A
p27
Relative p27 expression (%)
100
80
60
40
20
0
shRNA:
NS
#1
#2
p27
B
p27
NS
#1
#2
Mismatch
Imetelstat
C
Mismatch
Imetelstat
Cell viability (%)
100
80
60
40
20
0
shRNA:
NS
#1
#2
p27
D
Mismatch
Imetelstat
% Apoptosis
4.0
3.0
2.0
1.0
0.0
shRNA:
NS
#1
#2
p27
E
Mismatch
Imetelstat
Telomerase activity (%)
100
80
60
40
20
0
shRNA:
NS
#1
#2
p27
F
Mismatch
Imetelstat
Fold PUMA upregulation
4.0
3.0
2.0
1.0
0.0
shRNA:
NS
#1
#2
p27

**Fig. S6**

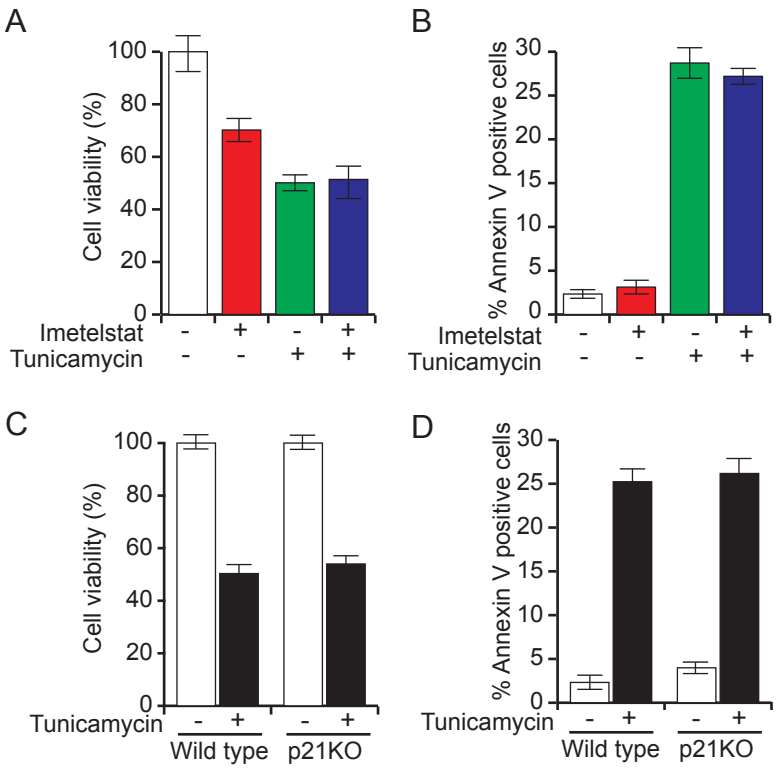
A
Cell viability (%)
100
80
60
40
20
0
Imetelstat - + - +
Tunicamycin - - + +
B
% Annexin V positive cells
30
25
20
15
10
5
0
Imetelstat - + - +
Tunicamycin - - + +
C
Cell viability (%)
100
80
60
40
20
0
Tunicamycin - + - +
Wild type
p21KO
D
% Annexin V positive cells
30
25
20
15
10
5
0
Tunicamycin - + - +
Wild type
p21KO

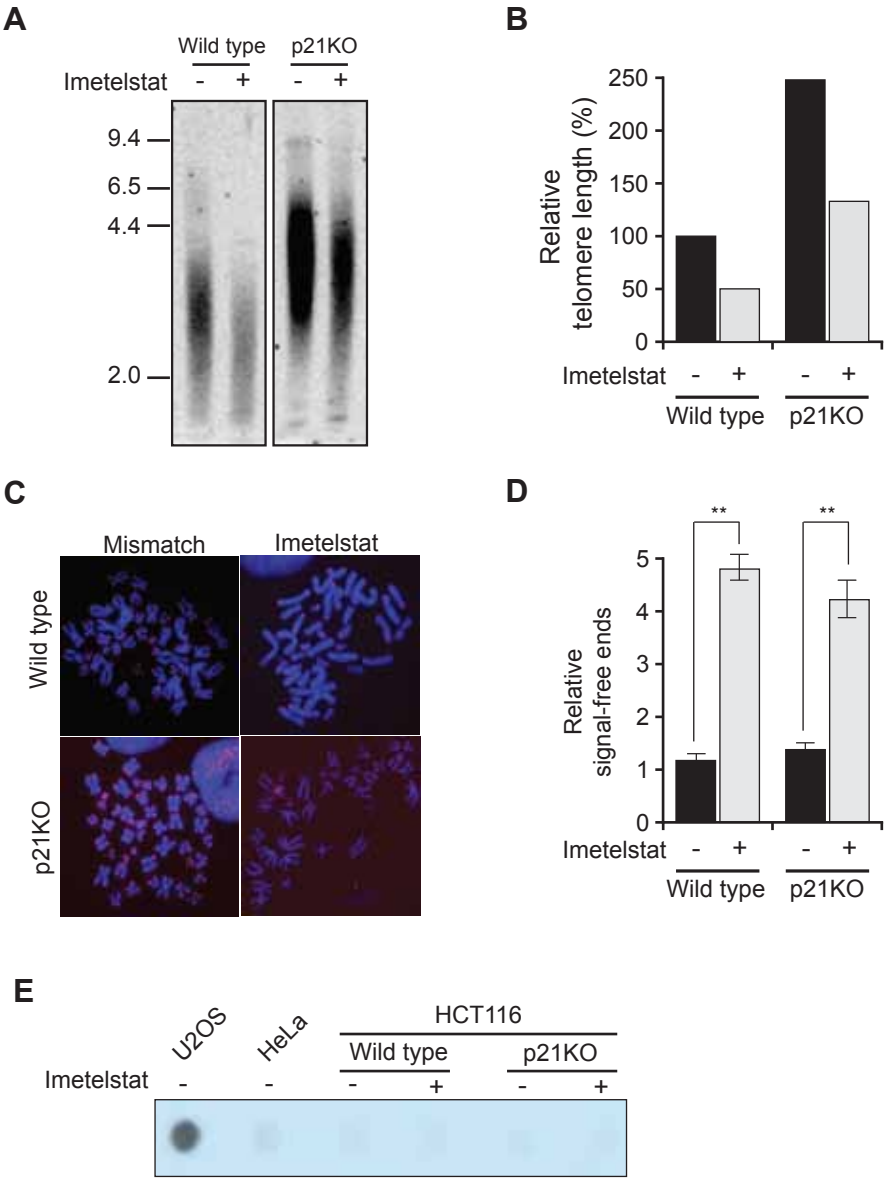
A
Wild type
p21KO
Imetelstat
- + - +
9.4
6.5
4.4
2.0
B
Relative telomere length (%)
250
200
150
100
50
0
Imetelstat - + - +
Wild type
p21KO
C
Mismatch
Imetelstat
Wild type
p21KO
D
Relative signal-free ends
**
**
5
4
3
2
1
0
Imetelstat - + - +
Wild type
p21KO
E
U2OS
HeLa
HCT116
Wild type
p21KO
Imetelstat
- - - + - +

**Fig. S8**

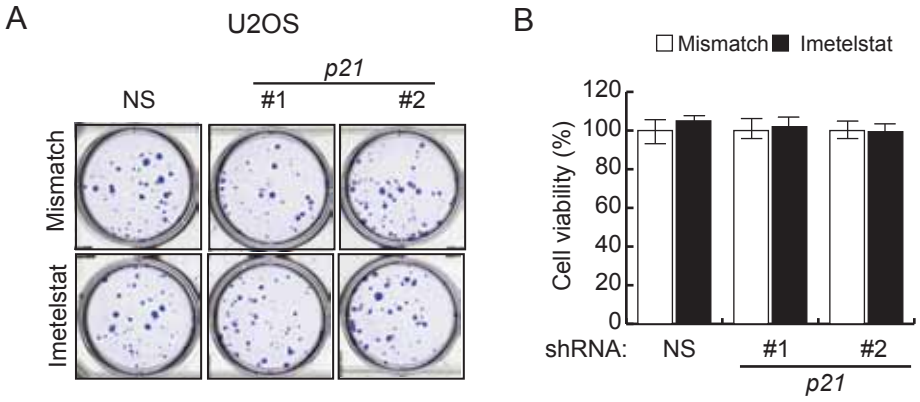
A
U2OS
p21
NS
#1
#2
Mismatch
Imetelstat
B
Mismatch
Imetelstat
Cell viability (%)
120
100
80
60
40
20
0
shRNA:
NS
#1
#2
p21

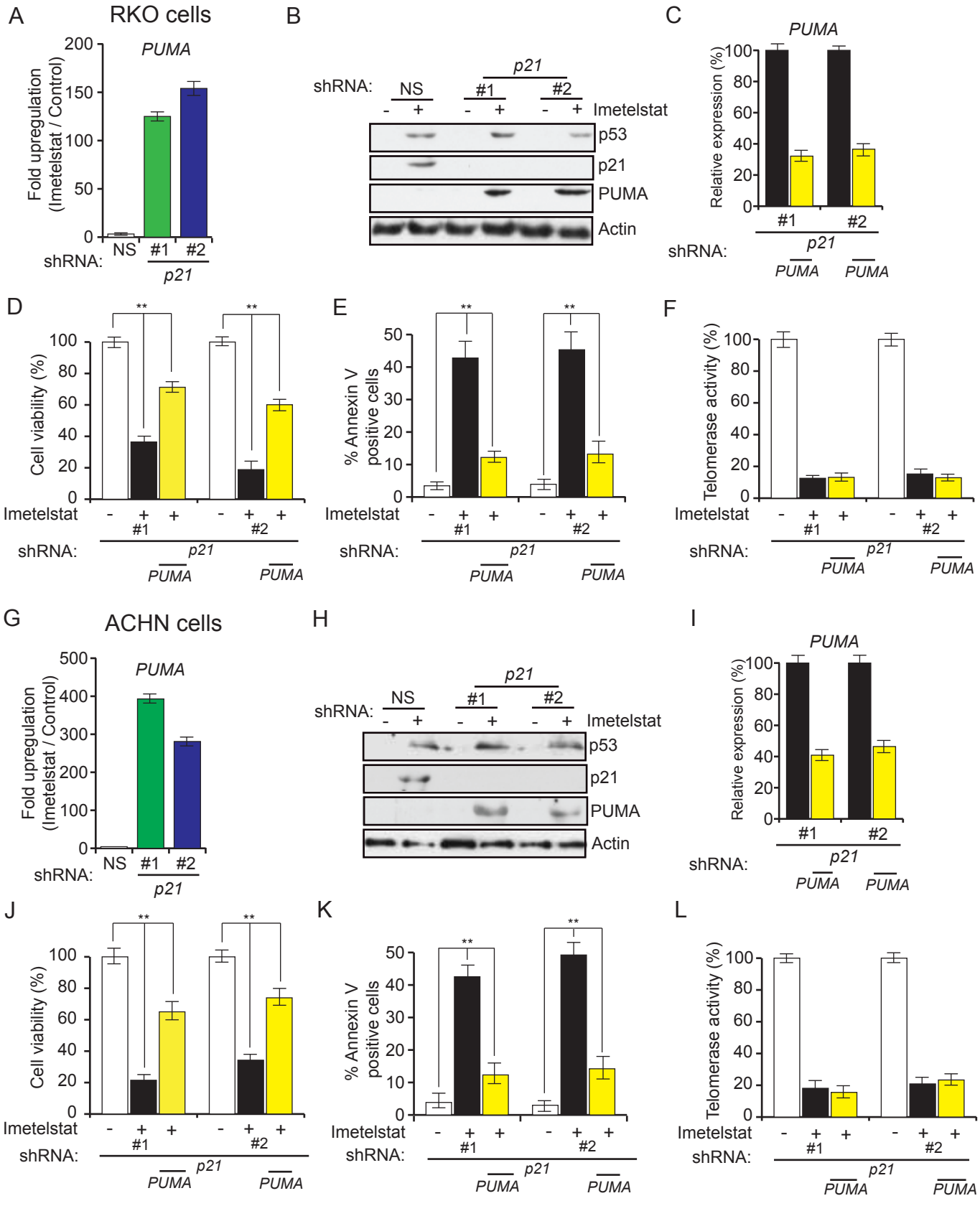
A
RKO cells
PUMA
Fold upregulation (Imetelstat / Control)
200
150
100
50
0
NS
#1
#2
shRNA:
p21
B
shRNA:
NS
p21
#1
#2
Imetelstat
p53
p21
PUMA
Actin
C
PUMA
Relative expression (%)
100
80
60
40
20
0
#1
#2
shRNA:
p21
PUMA
PUMA
D
Cell viability (%)
100
80
60
40
20
0
**
**
Imetelstat
shRNA:
#1
#2
p21
PUMA
PUMA
E
% Annexin V positive cells
50
40
30
20
10
0
**
**
Imetelstat
shRNA:
#1
#2
p21
PUMA
PUMA
F
Telomerase activity (%)
100
80
60
40
20
0
Imetelstat
shRNA:
#1
#2
p21
PUMA
PUMA
G
ACHN cells
PUMA
Fold upregulation (Imetelstat / Control)
500
400
300
200
100
0
NS
#1
#2
shRNA:
p21
H
shRNA:
NS
p21
#1
#2
Imetelstat
p53
p21
PUMA
Actin
I
PUMA
Relative expression (%)
100
80
60
40
20
0
#1
#2
shRNA:
p21
PUMA
PUMA
J
Cell viability (%)
100
80
60
40
20
0
**
**
Imetelstat
shRNA:
#1
#2
p21
PUMA
PUMA
K
% Annexin V positive cells
50
40
30
20
10
0
**
**
Imetelstat
shRNA:
#1
#2
p21
PUMA
PUMA
L
Telomerase activity (%)
100
80
60
40
20
0
Imetelstat
shRNA:
#1
#2
p21
PUMA
PUMA

**Fig. S10**

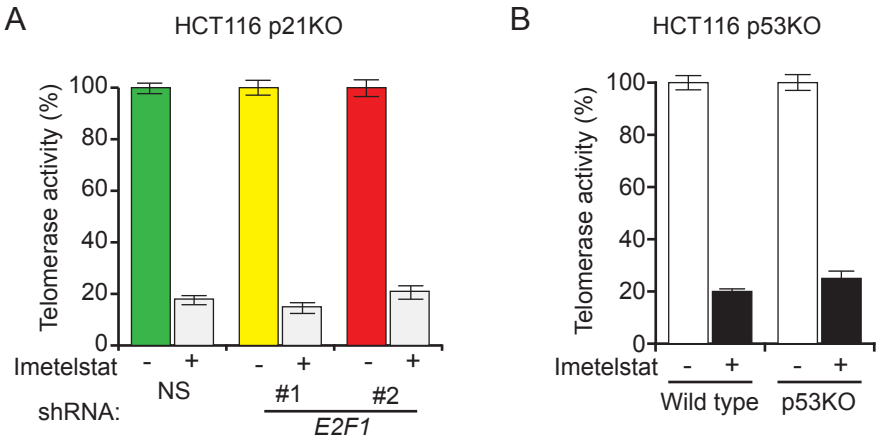
A
HCT116 p21KO
Telomerase activity (%)
100
80
60
40
20
0
Imetelstat
-
+
-
+
-
+
NS
#1
#2
shRNA:
E2F1
B
HCT116 p53KO
Telomerase activity (%)
100
80
60
40
20
0
Imetelstat
-
+
-
+
Wild type
p53KO

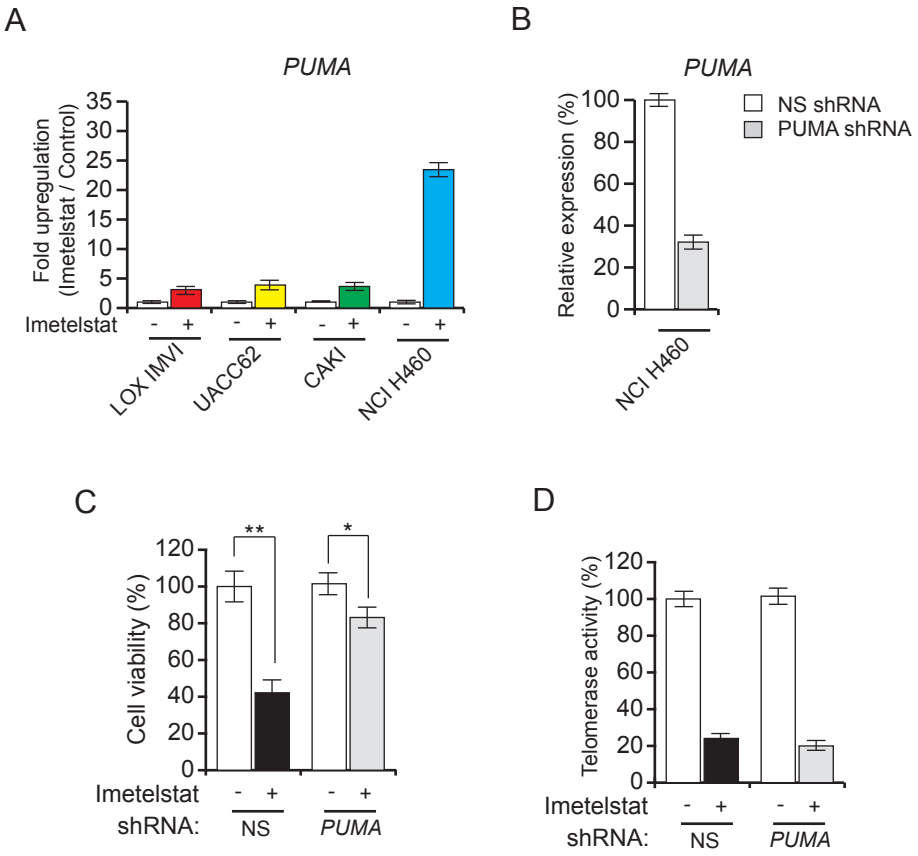
A
PUMA
Fold upregulation (Imetelstat / Control)
35
30
25
20
15
10
5
0
Imetelstat
- + - + - + - +
LOX IMVI
UACC62
CAKI
NCI H460
B
PUMA
Relative expression (%)
100
80
60
40
20
0
NS shRNA
PUMA shRNA
NCI H460
C
Cell viability (%)
120
100
80
60
40
20
0
**
*
Imetelstat
shRNA:
- + - +
NS
PUMA
D
Telomerase activity (%)
120
100
80
60
40
20
0
Imetelstat
shRNA:
- + - +
NS
PUMA

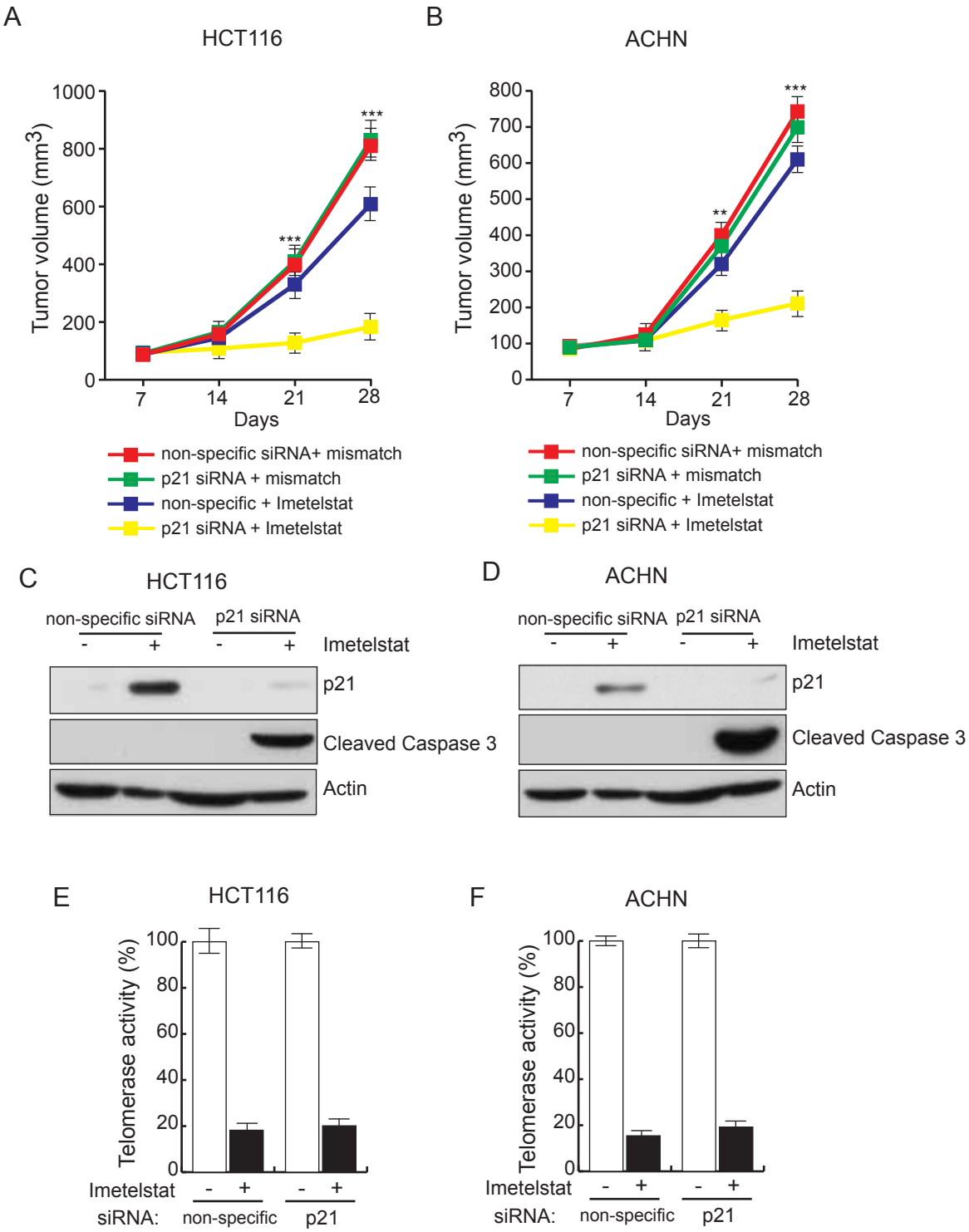
A
HCT116
Tumor volume (mm3)
Days
non-specific siRNA+ mismatch
p21 siRNA + mismatch
non-specific + Imetelstat
p21 siRNA + Imetelstat
B
ACHN
C
HCT116
non-specific siRNA
p21 siRNA
Imetelstat
p21
Cleaved Caspase 3
Actin
D
ACHN
E
HCT116
Telomerase activity (%)
siRNA:
non-specific
p21
F
ACHN

**Fig. S13**

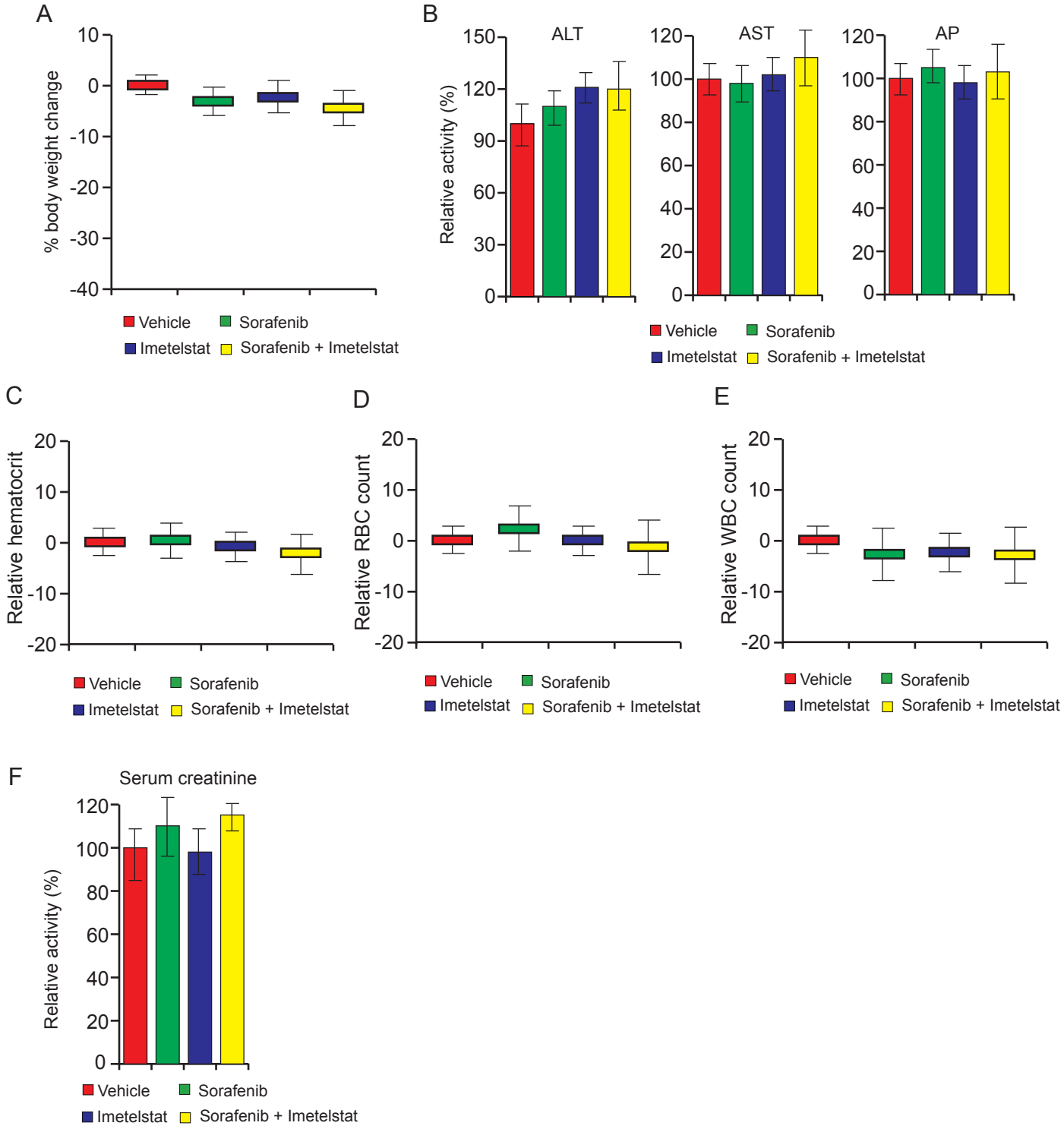
A
% body weight change
10
0
-10
-20
-30
-40
Vehicle
Sorafenib
Imetelstat
Sorafenib + Imetelstat
B
Relative activity (%)
ALT
AST
AP
150
120
90
60
30
0
100
80
40
20
Vehicle
Sorafenib
Imetelstat
Sorafenib + Imetelstat
C
Relative hematocrit
20
10
0
-10
-20
Vehicle
Sorafenib
Imetelstat
Sorafenib + Imetelstat
D
Relative RBC count
20
10
0
-10
-20
Vehicle
Sorafenib
Imetelstat
Sorafenib + Imetelstat
E
Relative WBC count
20
10
0
-10
-20
Vehicle
Sorafenib
Imetelstat
Sorafenib + Imetelstat
F
Serum creatinine
Relative activity (%)
120
100
80
60
40
20
0
Vehicle
Sorafenib
Imetelstat
Sorafenib + Imetelstat

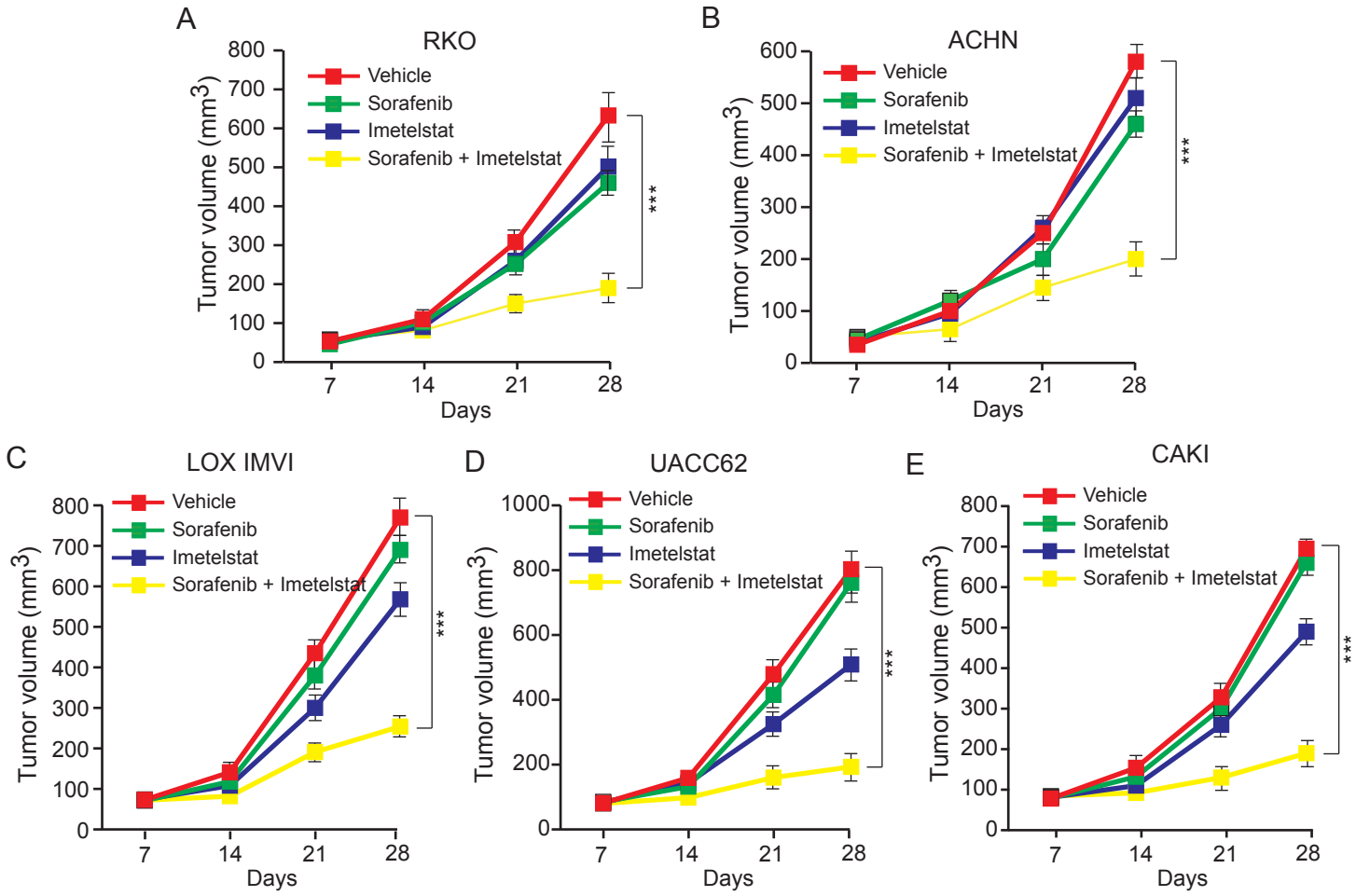
A
RKO
Vehicle
Sorafenib
Imetelstat
Sorafenib + Imetelstat
Tumor volume (mm3)
Days
***
B
ACHN
C
LOX IMVI
D
UACC62
E
CAKI

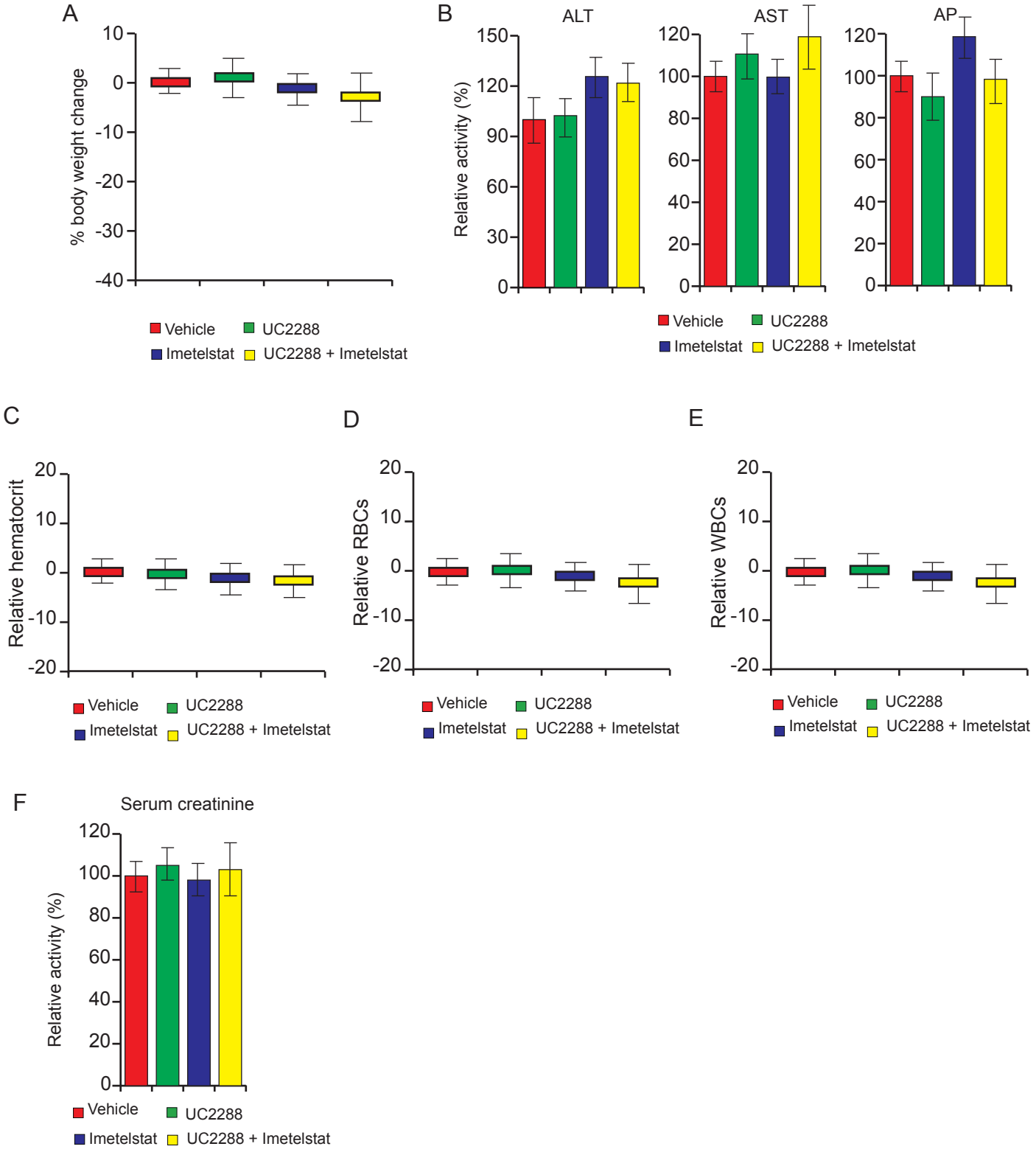
A
% body weight change
10
0
-10
-20
-30
-40
Vehicle
UC2288
Imetelstat
UC2288 + Imetelstat
B
ALT
AST
AP
Relative activity (%)
150
120
90
60
30
0
120
100
80
60
40
20
0
Vehicle
UC2288
Imetelstat
UC2288 + Imetelstat
C
Relative hematocrit
20
10
0
-10
-20
Vehicle
UC2288
Imetelstat
UC2288 + Imetelstat
D
Relative RBCs
20
10
0
-10
-20
Vehicle
UC2288
Imetelstat
UC2288 + Imetelstat
E
Relative WBCs
20
10
0
-10
-20
Vehicle
UC2288
Imetelstat
UC2288 + Imetelstat
F
Serum creatinine
Relative activity (%)
120
100
80
60
40
20
0
Vehicle
UC2288
Imetelstat
UC2288 + Imetelstat

**Fig. S16**

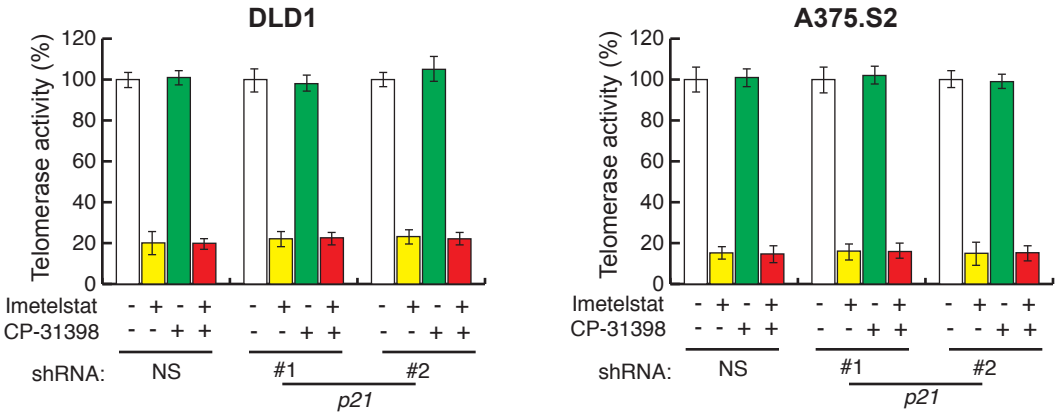
DLD1
A375.S2
Telomerase activity (%)
120
100
80
60
40
20
0
Imetelstat
CP-31398
shRNA:
NS
#1
#2
p21